Paleoceanography and Paleoclimatology

RESEARCH ARTICLE
10.1029/2024PA004927

Southern Ocean and Southern African Monsoon Forcing of the Subtropical Indian Ocean Early Pliocene "Biogenic Bloom"

D. N. Tangunan[1,2,3], J. A. Flores[1], L. J. LeVay[4], F. J. Jimenez-Espejo[5], J. J. Coenen[6], M. A. Berke[7], A. Q. de Azevedo[8], M. A. Fuertes[1], J. Gruetzner[9], A. Starr[2,10], and I. R. Hall[2]

[1]Departamento de Geología, Universidad de Salamanca, Salamanca, Spain, [2]School of Earth and Environmental Sciences, Cardiff University, Cardiff, UK, [3]Department of Earth Sciences, University College London, London, UK, [4]International Ocean Discovery Program, Texas A&M University, College Station, TX, USA, [5]Instituto Andaluz de Ciencias de la Tierra, Consejo Superior de Investigaciones Científicas, Universidad de Granada, Granada, Spain, [6]Department of Earth and Atmospheric Sciences, University of Nebraska-Lincoln, Lincoln, NE, USA, [7]Department of Civil and Environmental Engineering and Earth Sciences, University of Notre Dame, Notre Dame, IN, USA, [8]Instituto Oceanográfico, Universidade de São Paulo, Butantã, Brazil, [9]Alfred-Wegener-Institut for Polar and Marine Research, Bremerhaven, Germany, [10]Department of Geography, University of Cambridge, Cambridge, UK

Abstract The Pliocene epoch emerges as a pivotal juncture in Earth's climatic evolution, characterized by pronounced warmth and elevated atmospheric carbon dioxide compared to contemporary levels. While the broader climatic context of the Pliocene has garnered attention, there remains an outstanding gap in detailed paleoclimate reconstructions of the early Pliocene, a new potential target for data-model intercomparison. Addressing this, we investigate the drivers of the early Pliocene "Biogenic Bloom" and implications for nutrient dynamics and climate. By analyzing high-resolution biotic assemblage and geochemical records from the Agulhas Plateau, southwestern Indian Ocean (International Ocean Discovery Program, IODP Site U1475), we aim to elucidate the forcing and feedback mechanisms driving the early Pliocene marine ecosystems. We identify a distinct shift in coccolithophore assemblages at ∼4.6 million years ago, characterized by a notable change in dominance between the larger and smaller *Reticulofenestra* and high abundances of Noelaerhabdaceae < 5 μm. Our findings confirm the adaptive strategies of coccolithophore communities to prevailing environmental conditions, underscoring their evolutionary resilience by producing smaller coccoliths while increasing their abundances in a nutrient-replete ocean. Surface water dynamics, particularly the subtropical front migration and expansion of Southern Ocean waters, in combination with the southern African monsoon variability, emerge as key drivers of phytoplankton productivity during the early Pliocene. We posit that a weakened biological carbon pump, due to increased phytoplankton production driven by intense ocean circulation and mixing during the early Pliocene, served as a potential precursor to the subsequent middle Pliocene abrupt climate extremes.

Key Points:

- Expansion and leakage of cold, nutrient-rich Southern Ocean waters to the subtropical Indian Ocean occurred during the early Pliocene
- Intensification of southern African monsoon from ∼4.5 Ma impacted surface water carbonate production in the Agulhas Plateau
- The early Pliocene "biogenic bloom" can be considered as a potential precursor to the mid-Pliocene Warm Period

Supporting Information:

Supporting Information may be found in the online version of this article.

Correspondence to:

D. N. Tangunan,
d.tangunan@ucl.ac.uk

Citation:

Tangunan, D. N., Flores, J. A., LeVay, L. J., Jimenez-Espejo, F. J., Coenen, J. J., Berke, M. A., et al. (2024). Southern Ocean and southern African monsoon forcing of the subtropical Indian Ocean early Pliocene "Biogenic Bloom". *Paleoceanography and Paleoclimatology*, *39*, e2024PA004927. https://doi.org/10.1029/2024PA004927

Received 20 MAY 2024
Accepted 2 NOV 2024

Author Contributions:

Conceptualization: D. N. Tangunan, J. A. Flores, L. J. LeVay, F. J. Jimenez-Espejo, M. A. Berke, I. R. Hall
Data curation: D. N. Tangunan, L. J. LeVay, F. J. Jimenez-Espejo, J. J. Coenen, M. A. Berke, J. Gruetzner, I. R. Hall
Formal analysis: D. N. Tangunan, A. Q. de Azevedo
Funding acquisition: D. N. Tangunan, J. A. Flores
Investigation: D. N. Tangunan, L. J. LeVay, F. J. Jimenez-Espejo, J. J. Coenen, M. A. Berke, J. Gruetzner, I. R. Hall

1. Introduction

The Pliocene epoch (5.33–2.58 Ma) is a critical period in Earth's climate evolution. It records a significant transition from warm and stable conditions to the colder and highly variable Pleistocene climate (Filippelli & Flores, 2009; Lisiecki & Raymo, 2005). During this epoch, global temperatures were approximately 3°C warmer than present-day averages (Bartoli et al., 2011), with reduced ocean zonal temperatures (Fedorov et al., 2013), and a significantly expanded tropical warm pool (Brierley et al., 2009). Moreover, atmospheric carbon dioxide (pCO_2) levels ranged between 50 and 125 ppmv higher than the pre-industrial concentrations (∼400 ppmv) (Bartoli et al., 2011; Dowsett et al., 2013), with sea levels higher by ∼25 m than today (Dutton et al., 2015). Such pronounced near-modern climatic conditions, driven by ocean-atmosphere dynamics, gateway changes, and tectonic evolution (e.g., Brierley & Fedorov, 2016; Karas et al., 2017), render the Pliocene a crucial analogue for understanding current and impending climatic trajectories (Salzmann et al., 2011).

The early Pliocene (Zanclean stage; 5.3 to 3.6 Ma) is a particularly notable interval because it covers the later part of the globally documented late Miocene to early Pliocene "Biogenic Bloom" (∼9–3.5 Ma; Farrell et al., 1995), as well as the Early Pliocene Climatic Optimum (EPCO; 4.4 to 4.0 Ma). The term "biogenic bloom" is used here to

Methodology: D. N. Tangunan, L. J. LeVay, F. J. Jimenez-Espejo, J. J. Coenen, M. A. Berke, M. A. Fuertes, J. Gruetzner, A. Starr
Project administration: D. N. Tangunan, J. A. Flores
Resources: D. N. Tangunan, J. A. Flores, L. J. LeVay, I. R. Hall
Software: M. A. Fuertes
Supervision: J. A. Flores, I. R. Hall
Visualization: D. N. Tangunan, A. Q. de Azevedo
Writing – original draft: D. N. Tangunan
Writing – review & editing: D. N. Tangunan, J. A. Flores, L. J. LeVay, F. J. Jimenez-Espejo, J. J. Coenen, M. A. Berke, A. Q. de Azevedo, M. A. Fuertes, J. Gruetzner, A. Starr, I. R. Hall

represent broadly a sustained increase in biogenic export production and sedimentation (e.g., Dickens & Owen, 1999; Diester-Haass et al., 2005) and does not necessarily imply modern ecosystem dynamics. During the early Pliocene, a biogenic bloom was recorded across various locations in major ocean basins, including both upwelling and oligotrophic regions away from convergence zones (e.g., Dickens & Owen, 1999; Diester-Haass et al., 2005; Karatsolis et al., 2022; Lyle et al., 2019). Evidence for high phytoplankton production during this interval has been mainly linked to the accumulation rates of carbonate and biogenic silica in sediments (e.g., Dickens & Owen, 1999). These widespread phytoplankton blooms not only signify increased primary productivity but also have the potential to influence global carbon cycling dynamics.

Nutrient dynamics, particularly enhanced nutrient delivery, is central to initiating biogenic bloom events (Filippelli, 1997). For instance, the onset of the late Miocene to early Pliocene biogenic bloom has been attributed to various mechanisms affecting nutrient delivery into a particular region. Continental weathering from the uplift of the Himalayas and the intensification of the late Miocene Indian and Asian monsoons, along with associated upwelling events, have enhanced the nutrient supply to the Indian and Atlantic Oceans (e.g., Filippelli, 1997; Hermoyian & Owen, 2001), as well as to the marginal seas such as the South China Sea (L. Zhang et al., 2009). Changes in ocean-atmosphere dynamics, characterized by a shift of nutrients from oligotrophic regions toward divergence zones (Dickens & Owen, 1999), have also led to a significant redistribution of nutrients within ocean basins. In tropical regions, such as in the Indian and eastern Pacific Oceans, the biogenic bloom event has been linked to other factors, such as sea-level fluctuations (Diester-Haass et al., 2004), deep-water circulation intensification (Molnar et al., 2010), variations in trade wind patterns (Filippelli, 1997), and changes in upwelling intensities (e.g., Dickens & Owen, 1999; Diester-Haass et al., 2005). Understanding the timing and causal mechanisms of biogenic blooms is therefore of paramount importance as it may have primed the Earth's climate system and potentially paved the way for subsequent extreme warming intervals of the Pliocene (e.g., the mid-Pliocene Warm Period, mPWP).

The Indian-Atlantic Ocean Gateway (I-AOG) emerges as a critical focal point for understanding the complexities of the Pliocene climatic regime, as the interconnections between ocean water masses at both low and high-latitude regions are vital components of the Earth's climate system (Figure 1). Integral to this system is the Agulhas Current, the largest surface western boundary current in the Southern Hemisphere, which facilitates the transfer of approximately 70 Sverdrup of warm and saline surface waters from the Indian and Pacific Oceans to the Atlantic (Beal et al., 2011). This transfer, via the Agulhas Leakage, exerts significant influence on the Atlantic Meridional Overturning Circulation and climate of the North Atlantic on various timescales (Biastoch et al., 2009). Notably, the warm and saline Agulhas Current dominates the Indian sector of the Southern Ocean, where it interacts with the cold and fresh Southern Ocean water (Lutjeharms, 1996). Surface ocean nutrients in the I-AOG are primarily supplied by the northward advection and lateral mixing of the nutrient-rich southern-sourced Subantarctic Surface Water (SASW; Sigman et al., 1999), which in the past was closely associated with the subtropical front (STF) migration and/or the variability of the Southern Hemisphere westerlies (De Boer et al., 2013; Kohfeld et al., 2013). Paleoceanographic evidence, particularly from the Pleistocene and recent glacial stages, suggests that the changing position of the STF over glacial-interglacial cycles impacted surface ocean dynamics and drove nutrient availability and export production in the region (De Boer et al., 2013; Orsi et al., 1995). However, compared to the Pleistocene (e.g., Cartagena-Sierra et al., 2021; Romero et al., 2015; Tangunan et al., 2021), studies on the Pliocene migration of the STF in the I-AOG region are limited.

Past climatic and oceanographic variability in high latitude regions, such as the I-AOG can be evaluated by quantifying phytoplankton community changes (i.e., coccolithophores; coccoliths), comprising up to 20% of the phytoplankton carbon pool in pelagic regions (Poulton et al., 2007) and forming extensive blooms in modern higher latitudes (Balch et al., 2007). It has been shown that modern coccolithophores are sensitive to changes in sea surface temperature (SST), salinity, and nutrient supply across all latitudes (e.g., Winter et al., 1994). For example, in the Southern Ocean, the Polar Front separates the “Great Calcite Belt” dominated by coccolithophores to its north (Balch et al., 2016), and the “Circumpolar Silica Belt” established by diatoms to its south (Tréguer, 2002). The abundances and dynamics of these two phytoplankton groups in the Southern Ocean are essential for determining ecosystem responses to a changing marine environment, especially over timescales of enhanced biological production and extreme climatic conditions.

Coccolithophores constitute the foundation of the oceanic food chain and are unique because of their dual role in the global carbon cycle (e.g., Hay, 2004; Rost & Riebesell, 2004). This group affects the biological carbon pump

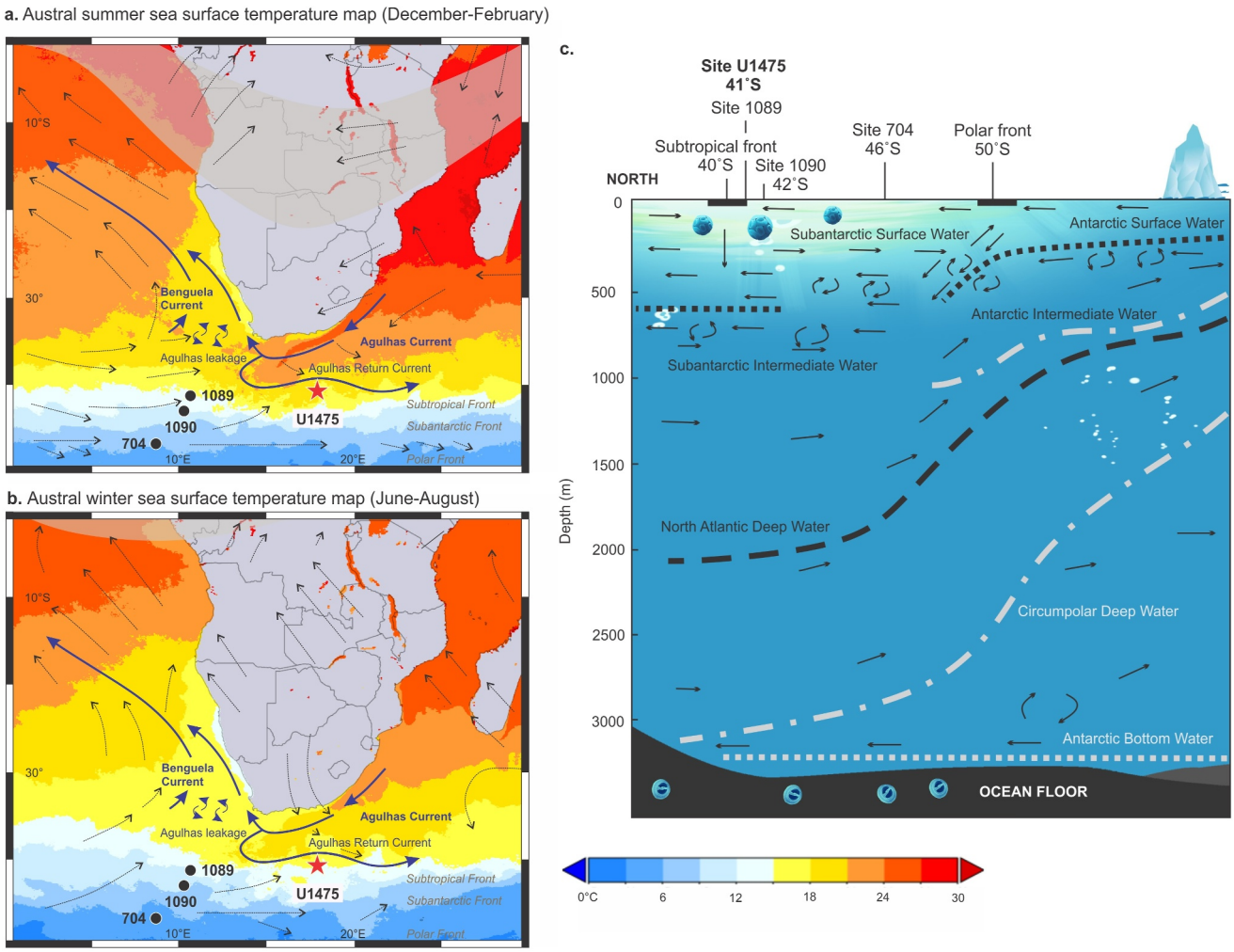

Figure 1. Key atmospheric and oceanographic features over South Africa and adjacent oceans, showing modern sea surface temperature (SST), surface and bottom water currents, and location of the investigated region (red star) and nearby sites mentioned in text (black circles). (a) SST averaged for December 2020 to February 2021 and prevailing winds during austral summer. (b) SST averaged for June–August 2021 and prevailing winds during austral winter. The zone of intertropical convergence is marked as a shaded band. The Southern Ocean frontal systems are also indicated: subtropical front, subantarctic front, and polar front showing northward migration during austral winter. (c) schematic north-south transect of the subtropical South Atlantic with the distribution of water masses. SST maps were generated with the Giovanni online data system developed and maintained by the NASA GES DISC (Acker & Leptoukh, 2007). Prevailing winds were drawn after Dickson et al. (2010). The cross-section image was redrawn and modified from Hodell and Venz (1992).

(BCP) by influencing both the soft-tissue pump (STP, via photosynthesis) and the calcium carbonate counter pump (CCP, via calcification) (Hay, 2004). The relationship between water mass properties (e.g., temperature, salinity, stratification) and phytoplankton communities controls the efficiency of the BCP (Villa et al., 2014). The reconstruction of biological production and calcification patterns associated with BCP efficiency in subtropical regions has primarily focused on more recent timescales such as the Pleistocene and the latest interglacial period (e.g., Brandon et al., 2022; Duchamp-Alphonse et al., 2018). The availability of new International Ocean Discovery Program (IODP) sites extending back through the Pliocene now offers an unprecedented opportunity to explore the early Pliocene warmth in the I-AOG and its implications for ocean circulation, nutrient cycling, and climate dynamics.

Drilling at IODP Site U1475 (Agulhas Plateau; 41°25.61′S; 25°15.64′E; water depth of 2,669 m) located in the Indian sector of the Southern Ocean (Figure 1) recovered a continuous carbonate-rich succession spanning the last 7 Ma (Hall et al., 2017b). This allows unsurpassed resolution covering the whole Pliocene epoch, offering an opportunity to investigate the early Pliocene biogenic bloom event. Here, we present high-resolution biotic assemblage and morphometric records, combined with bulk calcium carbonate and biogenic silica, and elemental

geochemistry records, to determine both the forcing and feedback mechanisms of the early Pliocene marine ecosystems. Our study provides comprehensive insights into the potential significant impacts of the interplay between biotic communities, carbon cycling dynamics, and global climatic shifts during the early Pliocene.

2. Regional Oceanographic Setting

IODP Site U1475, situated on the southwestern Agulhas Plateau, lies at a critical juncture between the Indian, Southern, and Atlantic Oceans (Figure 1; Hall et al., 2017b). The Agulhas Plateau is bathed by the southward propagating North Atlantic Deep Water and the northward flowing southern-sourced Antarctic Intermediate Water and Antarctic Bottom Water (Figure 1c; Reid, 2005). This site is influenced significantly by the Agulhas Current system, which forms a crucial part of the meridional overturning circulation and acts as a primary pathway for transporting water from the Indian and Pacific Oceans to the Atlantic Ocean (Lutjeharms, 2006). The upper ocean hydrographic conditions over the Agulhas Plateau are primarily influenced by the interaction between the ARC, which carries warm and salty subtropical Indian Ocean surface waters via the Agulhas Current (Figures 1a and 1b), and the cold, fresh SASW south of the STF (Figure 1c; Lutjeharms, 2006). Seasonal SSTs at the site range from 11 to 17°C and salinities from 35.1 to 35.4 (Holliday & Read, 1998). During austral summer, the southward shift of the Inter Tropical Convergence Zone creates a north-south pressure gradient, intensifying moisture flux over southern Africa and bringing heavy rains through the southern African monsoon, a component of the Southern Hemisphere monsoon system (Clark et al., 2003; Xulu et al., 2020). This seasonal shift, influenced by the southern African monsoon alters hydrographic conditions by increasing precipitation and river discharge, reducing salinity, and enhancing stratification (Ma et al., 2021; Schott et al., 2009). The biological response to these oceanographic conditions is marked by seasonal variations in phytoplankton distribution, with coccolithophores showing high concentrations between the STF and the Subantarctic Front during austral summer, shifting up to ∼10° latitude northward during austral winter. Diatoms concentrate in the Subantarctic Zone during summer and disperse further north, up to ∼30°S, as their abundance decreases in winter (Gregg & Rousseaux, 2014; Patil et al., 2017).

3. Materials and Methods

3.1. Site U1475

IODP Site U1475 was recovered from the southwestern flank of the Agulhas Plateau (Figure 1; Hall et al., 2017b). The drilled sediments are part of a contourite drift (Gruetzner et al., 2019), characterized by pale brown and olive gray to light gray coccolith-rich foraminifera ooze (Unit I, 0–4.75 m cored depth below seafloor method A, CSF-A) and light greenish gray to light gray nannofossil ooze (Unit II, 4.75–277.22 m CSF-A) (Hall et al., 2017b). Site U1475 represents a ∼256-m-long continuous sequence of late Miocene to late Pleistocene sediments. Samples for this study were taken with a mean sampling resolution of ∼10 kyr from the early Pliocene section (4.95–3.30 Ma) of the stratigraphic splice. A total of 162 samples were analyzed for complete coccolith assemblage composition, with 17 of these samples further analyzed for morphometry. Initial shipboard investigation showed relatively good preservation of coccolith species, especially the placolith-bearing taxa belonging to the Noelaerhabdaceae family. Shipboard analysis also recorded frequent occurrences of reworked Eocene to middle Miocene species like *Chiasmolithus* spp., *Cyclicargolithus abisectus*, *Cyclicargolithus floridanus*, *Dictyococcites bisecta*, *Reticulofenestra umbilica*, *Discoaster* spp., and *Isthmolithus recurvus*.

3.2. Chronology of Site U1475

The initial Site U1475 chronology was based upon the shipboard age model established using combined biostratigraphy (calcareous nannofossils, planktic foraminifera, diatoms) and magnetostratigraphy (Hall et al., 2017b). The shipboard age model was refined by aligning the shipboard physical properties records (Gruetzner et al., 2019) to the global benthic foraminifera (Lisiecki & Raymo, 2005) and probabilistic (Ahn et al., 2017) stacks (Table S1 and Figure S1 in Supporting Information S1). While the generated age model is considered robust, the absence of high-resolution benthic isotope stratigraphy for this interval does not permit a detailed analysis of individual glacial-interglacial episodes, and conclusions have been considered with this limitation in mind.

3.3. Coccolith Taxonomy, Abundance, and Preservation

Slides for coccolith analysis were prepared following the standard random settling technique (Flores & Sierro, 1997). Counting was performed using a Nikon Eclipse 80i petrographic microscope under transmitted light in cross-polarized and phase-contrast, at 1,000x magnification. Species taxonomic identification was based on the electronic guide to biodiversity and taxonomy of coccolithophores (Nannotax 3; http://www.mikrotax.org/Nannotax3/). In this study, we grouped the *Reticulofenestra* species into four size classes: Group A = <3 μm and Group B = 3–5 μm (herein referred to as smaller *Reticulofenestra*), and Group C = 5–7 μm and Group D = >7 μm (herein referred to as larger *Reticulofenestra*). *Coccolithus pelagicus* morphotypes *C. pelagicus pelagicus* (<10 μm; herein referred to as *C. pelagicus*) and *C. pelagicus braarudii* (>10 μm; herein referred to as *C. braarudii*) are based on descriptions in Parente et al. (2004). We did not identify the larger *C. pelagicus* morphotype (*C. pelagicus azorinus*, >13 μm) in the samples. Further description of the *Reticulofenestra* taxonomic concept and ecological preferences can be found in Text S1 in Supporting Information S1.

Abundances were determined by counting at least 400 coccoliths per sample in various fields of view (FOV). Reworked species were counted but disregarded from the total abundance counts. An additional 10 to 20 FOV were counted to document less abundant coccolith taxa. The counts were then converted to absolute numbers (coccolith abundance, CA; coccoliths g^{-1} dry sediment) and the coccolith accumulation rates (CARs) were calculated by multiplying CA with the estimated sedimentation rate and the shipboard dry bulk density (DBD; Flores & Sierro, 1997). After counting, the entire slide was scanned to detect index taxa to refine biostratigraphy and confirm biostratigraphic boundaries. Coccolith preservation in each sample was assessed qualitatively while counting, using preservation criteria based on the degree of dissolution, fragmentation, and overgrowth (Hall et al., 2017a). Despite some evidence of reworking, coccolith specimens are generally of good to excellent preservation.

3.4. Morphometric Measurements

Seventeen slides were analyzed for morphometric parameters, such as the lengths of the major and minor axes, mass, and volume of the *Reticulofenestra* coccolith calcite using the C-calcita software. *Reticulofenestra* coccoliths appear fully visible when circularly polarized light is used, as they are formed by r-unit calcite crystals (radially oriented c-axis) without appreciable v-unit elements (vertically oriented c-axis) (Young et al., 2004). About 50 to 60 FOV photographs were taken using Nikon DS-Fil 8-bit color digital camera installed on the Nikon Eclipse LV100 polarizing microscope equipped with circular polarization (camera resolution scale = 1 pixel per 0.035 μm). Individual calcite particles (coccoliths) between 2 and 12 μm were automatically selected using the C-calcita software (Fuertes et al., 2014). From the generated output images, a minimum of 100 *Reticulofenestra* coccoliths for the size classes ≤5 μm (Groups A and B) and 50 for the size classes ≥5 μm (Groups C and D) per sample were selected manually after visual evaluation. All morphometric parameters are reported as averages.

The size-normalized thickness of *Reticulofenestra* coccoliths was calculated using the equation from O'Dea et al. (2014), which relates coccolith mass to changes in calcification. The formula incorporates mean coccolith length, individual coccolith length, and the regression slope between coccolith length and thickness. Coccolith carbonate mass accumulation rates (MAR) were derived by combining coccolith mass with sedimentation rate and DBD. The *k* value, indicating coccolith shape change and calcification intensity, was determined by dividing mass by the product of 2.7 (calcite density in pg/μm³) and the cube of length. To assess the relationship between calcification and photosynthesis, the particulate inorganic to organic carbon (PIC/POC) ratio was calculated based on Jin et al. (2018). This ratio reflects the cell size-adjusted calcite content of coccolithophores. Details on these methodologies can be found in Text S2 in Supporting Information S1.

3.5. Bulk Calcium Carbonate

Calcium carbonate weight percent ($CaCO_3$ wt. %) at Site U1475 was analyzed on 249 samples. All samples were oven-dried for at least 24 hr at 50°C before grinding and then dried in the oven for another 24 hr. $CaCO_3$ was estimated using a UIC Inc. model 5011 CO_2 coulometer. Dried powdered sediment (10–18 mg) was weighed on a microbalance and allowed to react with 2 M HCl. The resulting CO_2 was titrated, and the endpoint was determined by a photodetector. The escaped CO_2 was assumed to be entirely from dissolved $CaCO_3$. The total inorganic carbon output was given in mg C, and the following equation was used to calculate $CaCO_3$ wt. %: $CaCO_3$ wt. % = TIC (μg C) × 8.33/sample mass (μg C). A replicate was run after every five sample

measurements, and a standard (100% $CaCO_3$) was run after every 10 measurements to check for instrument drift. Calcium carbonate MARs were calculated by multiplying $CaCO_3$ wt. % with the estimated sedimentation rate and the shipboard DBD.

3.6. Bulk Biogenic Silica

Biogenic silica weight percent (BSi wt. %) was analyzed on 74 samples using a modified version of the Mortlock and Froelich (1989) method. Samples were freeze-dried and weighed (~55 mg) for further processing. To expose the opal surface and remove organics and carbonate from the samples, sediments are processed using 30% hydrogen peroxide and 1-M hydrochloric acid. With the organics and carbonates removed, the samples were introduced to a weak base (sodium carbonate 10%) and placed in an 80°C oven for 5 hr to break down the opal. Samples were then processed to determine opal percentage using a modified molybdate-blue spectrophotometer. Each sample run was processed with standards that ranged from 0 to 50 ppm in 5 ppm intervals.

3.7. X-Ray Fluorescence Measurement

The ~256-m-long stratigraphic splice from Site U1475 was scanned using a third-generation Avaatech Core Scanner with a Canberra X-PIPS SDD, Model SXD 15C-150–500 150 eV resolution X-ray detector. Before scanning, all core sections were scraped to clean the split core surface and covered with 4 μm–thick Ultralene plastic film (SPEX Centriprep, Inc.). X-ray fluorescence (XRF) data were collected every 3 cm downcore in three separate runs using generator settings of 10 kV/0.25 mA (no filter), 30 kV/1.25 mA (Pd-filter) and 50 kV/1.5 mA (Cu-filter), respectively. With the 10 kV setting, elements in the range from Al to Fe are detected, while at 30 kV, elements Rb, Sr and Zr are best resolved. Ba was measured with the 50 kV setting. In this study, only ratios of Al, Ca, Sr, and K are reported.

We used ln Fe/Ca and ln [(Al + K)/Ca] ratios as proxies to study terrigenous flux and monsoon dynamics (Gebregiorgis et al., 2020). The Fe/Ca ratio is based on the assumption that iron (Fe) in marine sediments is directly associated with terrigenous materials transported to the ocean by rivers and/or wind, while variations in calcium (Ca) levels indicate changes in the production of $CaCO_3$ by marine plankton (Caley et al., 2018). Similarly, the ln [(Al + K)/Ca] (Auer et al., 2019) ratio is sensitive to changes in terrestrial input versus marine productivity. Aluminum (Al) and potassium (K) are primarily found in terrestrial sediments, indicating the influx of material from land. During intensified monsoon or precipitation activity, terrestrial material (Fe, Al, K) transported to the ocean increases, raising the ratio, while marine productivity signals (Ca) may be relatively diluted (e.g., Auer et al., 2019; Clift et al., 2022; Gebregiorgis et al., 2020). Therefore, higher Fe/Ca and (Al + K)/Ca ratios indicate increased terrestrial fluxes due to intensified monsoon activity, whereas lower values suggest reduced terrestrial input and weaker monsoon periods.

3.8. Cyclostratigraphy

The time series data for bulk $CaCO_3$, *Florisphaera profunda* stratification index, and XRF elemental ratios were pre-processed by linearly interpolating the values to achieve equally spaced time intervals of 5.03 kyr for $CaCO_3$, 8.52 kyr for the *F. profunda* index, and 0.29 kyr for the elemental ratios. All the interpolated data series were detrended by removing 35% of the data to eliminate the long-term trend (Cleveland, 1979) by rLOESS (robust locally estimated scatterplot smoothing) smooth curve. The rLOESS method was used to fit a smooth curve to the data, which helps in identifying and removing these long-term trends, thus allowing for a more accurate analysis of the underlying patterns and short-term fluctuations in the data sets. All cyclostratigraphic and spectral analyses of the detrended data were performed using the Acycle software package (Li et al., 2019), a comprehensive tool for time series analysis and cyclostratigraphy that supports various statistical and visualization techniques. The dominant cyclicities and their statistical significance were analyzed using the multitaper method power spectral analysis (Thomson, 1982), which employs multiple orthogonal tapers to improve spectral estimates and minimize spectral leakage, providing a high-resolution view of frequency components in the data. Additionally, a robust red noise modeling procedure (Mann & Lees, 1996) was employed to distinguish true cyclic signals from background noise by fitting the observed spectrum to a red noise model, thus enhancing the detection of significant spectral peaks above the noise background. Peaks exceeding the 95% confidence level in the spectral analysis were cross-referenced with astronomical frequencies derived from the La2004 solution (Laskar et al., 2011). We then applied Fast Fourier transform (Kodama & Hinnov, 2014) to the data series to determine the evolution of orbital

frequencies through geologic time. A sliding-window of 200 kyr was applied to $CaCO_3$, 350 kyr to Fe/Ca, and 400 kyr to *F. profunda* index and ln [(Al + K)/Ca)].

4. Results

4.1. Biological Proxies: Coccolithophore Assemblage and Morphometry

Coccolithophore assemblages at Site U1475 consist of a mixture of tropical and subtropical taxa, with 25 identified species and species groups. Generally, the assemblages are dominated by species belonging to the genus *Reticulofenestra* with different size-defined morphotypes (<3 μm to >7 μm). All the *Reticulofenestra* sizes together comprise relative abundances between 40% and 90% of the total assemblages, and therefore reflect the main patterns of the total coccoliths (Figures 2a and 2b). Total coccolith absolute abundances range from 6.4×10^8 to 9.7×10^9 coccoliths g^{-1} dry sediment (Figure 2d), with *Reticulofenestra* abundances varying between 2.3×10^8 and 6.8×10^9.

During the early Pliocene, *Reticulofenestra* at Site U1475 features distinct variability in size classes (please refer to size classification described in Section 3.3), showing a general three-step shift between larger and smaller species (Figures 2a and 2b). In particular, the largest size class, Group D (>7 μm), shows the highest abundance from 4.95 to 4.6 Ma, decreases from 4.6 to 4.2 Ma, and almost completely disappears and replaced by the smaller size classes, Groups A (<3 μm) and B (3–5 μm) from 4.2 to 3.3 Ma. This stepwise change is also observed in the abundances of other coccolithophore taxa (e.g., *C. pelagicus*, *C. braarudii*, *F. profunda*; Figures 2e and 2f). We, therefore, subdivide the results based on these three time intervals, with the EPCO being discussed separately due to its distinct character.

4.1.1. Interval 4.95 to 4.6 Ma (I)

The interval between 4.95 and 4.6 Ma records the lowest abundances of smaller Noelaerhabdaceae species (<5 μm) (30%–65%), which are composed of *Reticulofenestra* and all species of *Gephyrocapsa* (Figure 2c). Alternatively, the larger *Reticulofenestra* registers the highest abundances (up to 44%; Figure 2b), with a concomitant increase in *C. braarudii* abundance (Figure 2f). A distinct peak in the abundance of the cooler water taxon *C. pelagicus* is recorded at ~4.8 Ma (27%), coinciding with low *F. profunda* abundance (Figure 2e), and a slight increase in Noelaerhabdaceae < 5 μm (Figure 2c).

4.1.2. Interval 4.6 to 4.4 Ma (II)

This interval is characterized by a pronounced shift from larger to smaller *Reticulofenestra* starting at 4.6 Ma (Figure 2a). *F. profunda* abundances show three distinct low intervals from 4.6 to 4.4 Ma (Figure 2e). This is accompanied by increases in both *C. braarudii* and *C. pelagicus*, and consistent high abundances of Noelaerhabdaceae <5 μm until 4.45 Ma (66%–91%). A steep reduction in Noelaerhabdaceae <5 μm is recorded from 4.45 to 4.4 Ma (Figure 2c).

4.1.3. Interval 4.4 to 4.0 Ma (III; Early Pliocene Climatic Optimum)

The onset of the EPCO at 4.4 Ma indicates recovery of the Noelaerhabdaceae < 5 μm (Figure 2c) and a drop in *F. profunda* abundances (Figure 2e). Noelaerhabdaceae <5 μm and *C. pelagicus* spp. (Figure 2f) abundances exhibit weak variability and remain stable throughout this period, with a notable decline in Noelaerhabdaceae <5 μm at 4.2 Ma.

4.1.4. Interval 4.0 to 3.3 Ma (IV)

After a sharp drop at the end of the EPCO, Noelaerhabdaceae <5 μm registers an increase in abundances from 4.0 Ma, with low variability until 3.3 Ma (58%–82%; Figure 2c). *C. pelagicus* spp. abundances remain low between 4.0 and 3.6 Ma (3%–8%; Figure 2f). From 3.6 Ma, increased abundances of *C. pelagicus* are recorded (up to 8.9%), along with increases in Noelaerhabdaceae <5 μm (61%–73%) and a reduction in *F. profunda* (3%–10%; Figure 2e).

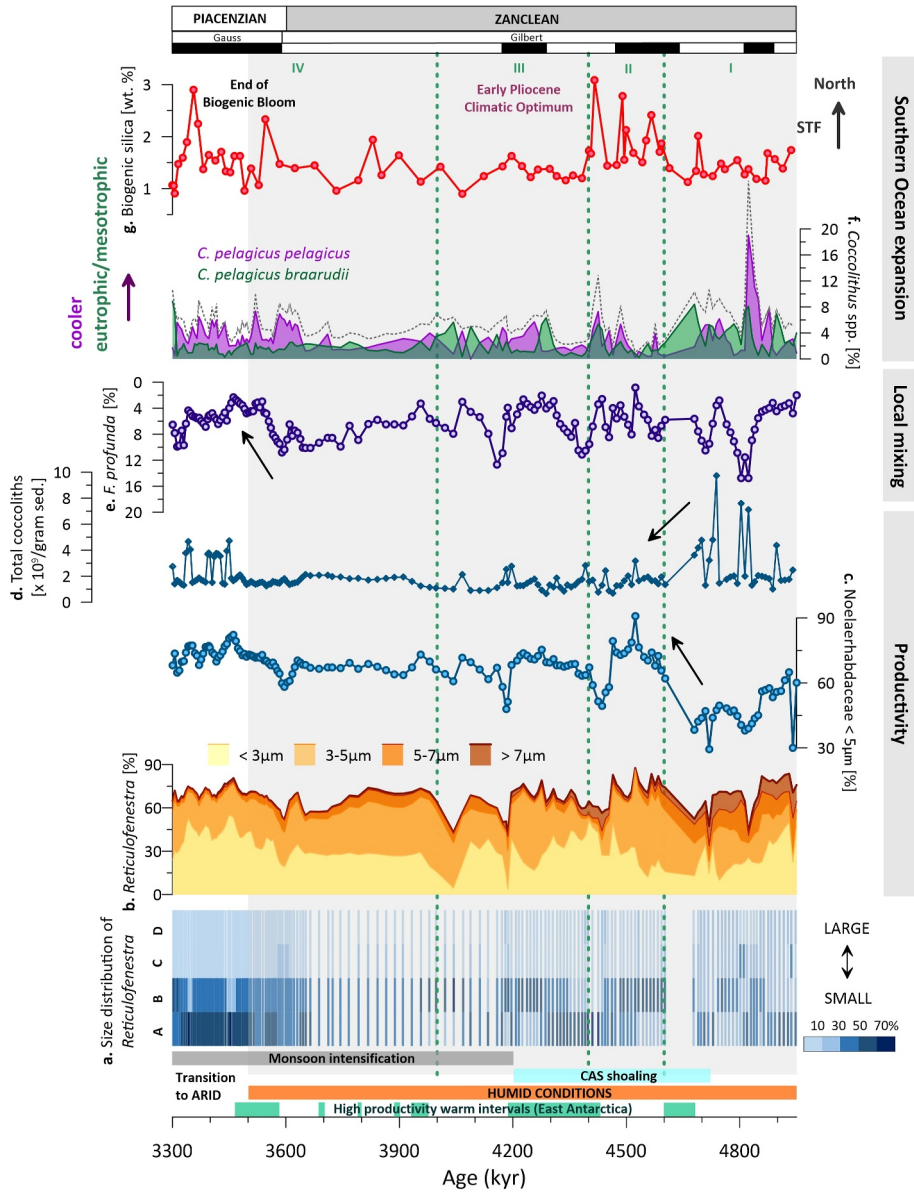

Figure 2. Site U1475 biological proxies reflecting early Pliocene ocean conditions in the Indian sector of the Southern Ocean. (a) Size distribution of *Reticulofenestra* coccoliths (*A* = <3 µm, *B* = 3–5 µm, *C* = 5–7 µm, *D* = >7 µm), (b) *Reticulofenestra* coccolith size fractions, (c) Noelaerhabdaceae <5 µm, (d) Total coccolith absolute abundance, (e) *Florisphaera profunda*, (f) *Coccolithus pelagicus* (*Coccolithus pelagicus* <10 µm, *Coccolithus braarud*ii >10 µm, total *C. pelagicus* spp. dotted dark gray), (g) Biogenic silica wt. %. Significant paleoceanographic events are indicated: Central American Seaway shoaling (Bell et al., 2015), monsoon intensification (Y. G. Zhang et al., 2009), high productivity warm intervals in East Antarctica (Cook et al., 2013), transition from humid to arid conditions (Christensen et al., 2017), and the later part of the late Miocene to early Pliocene biogenic bloom event (gray bar). Intervals I to IV (green dotted line and text) refer to the intervals discussed in the text.

4.1.5. *Reticulofenestra* Morphometry

Reticulofenestra analyzed for morphometric characteristics focused on four size groups: A (<3 µm), B (3–5 µm), C (5–7 µm), and D (>7 µm). The examined specimens have lengths ranging from 2 to 11.9 µm, with average lengths per sample between 3.2 and 7.2 µm (Figure 3). The morphometric records also reflect the stepwise trend observed in the overall coccolithophore abundances. Coccoliths are larger and heavier from 4.95 to 4.6 Ma (4.3–7.2 µm length; 54–143 pg mass) and are smaller and lighter from 4.6 to 3.3 Ma (3.2–5.2 µm length; 23–106 pg mass) (Figures 3b–3d). There is a strong correlation between length and mass (r = 0.88) throughout the studied

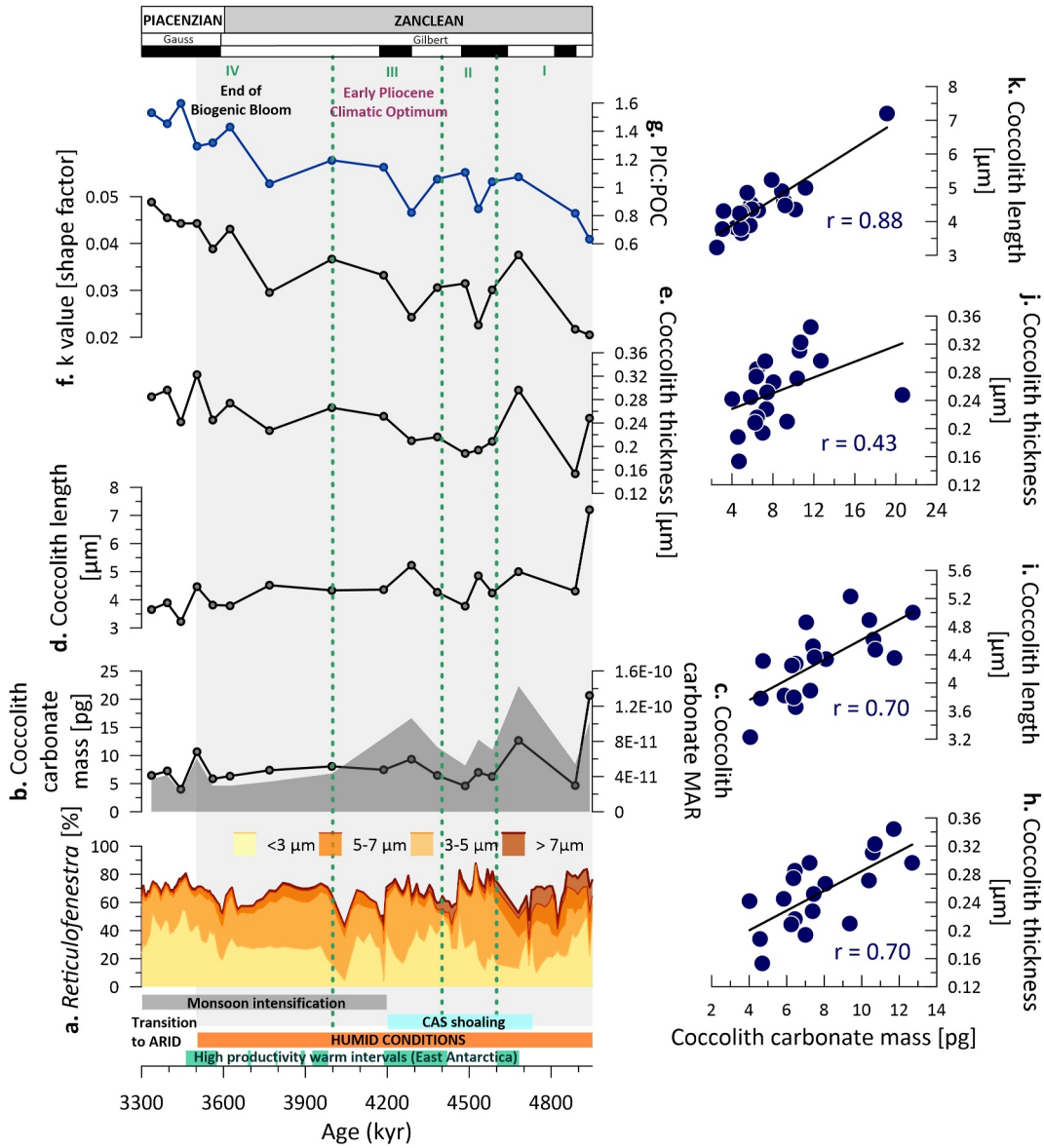

Figure 3. *Reticulofenestra* coccolith morphometric parameters and relative abundances at Site U1475. (a) Size distribution of *Reticulofenestra* coccoliths (A = <3 µm, B = 3–5 µm, C = 5–7 µm, D = >7 µm), averages of (b) coccolith carbonate mass (black line), (c) coccolith mass accumulation rate (MAR; g/cm^2/kyr; gray area), (d) coccolith length, (e) coccolith thickness, (f) k value (shape factor), (g) ratio between particulate inorganic and organic carbon (PIC/POC), h–k. relationship between the average coccolith carbonate mass and (h) Thickness and (i) length of *Reticulofenestra* ≤5 µm, (j) Thickness, and (k) length of all *Reticulofenestra* size classes. Significant paleoceanographic events are indicated: Central American Seaway shoaling (Bell et al., 2015), monsoon intensification (Y. G. Zhang et al., 2009), high productivity warm intervals in East Antarctica (Cook et al., 2013), transition from humid to arid conditions (Christensen et al., 2017), and the later part of the late Miocene to early Pliocene biogenic bloom event (gray bar). Intervals I to IV (green dotted line and text) refer to the intervals discussed in the text.

interval (Figure 3k) while mass and thickness have a lower correlation (r = 0.43) (Figure 3j). From 3.6 Ma, an interval dominated by smaller *Reticulofenestra*, it appears that thickness is not significantly correlated with either length or mass. A stronger correlation between mass and thickness (r = 0.70) (Figure 3h) and mass and length (r = 0.70) (Figure 3i) exists in *Reticulofenestra* ≤5 µm. Size-normalized coccolith thickness ranges between 0.15 and 0.34 µm (Figure 3e). Thickness shows a generally increasing pattern from 4.95 to 3.3 Ma with a k value of 0.02–0.05 (Figure 3f) and a PIC/POC ratio of 0.63–1.60 pg (Figure 3g).

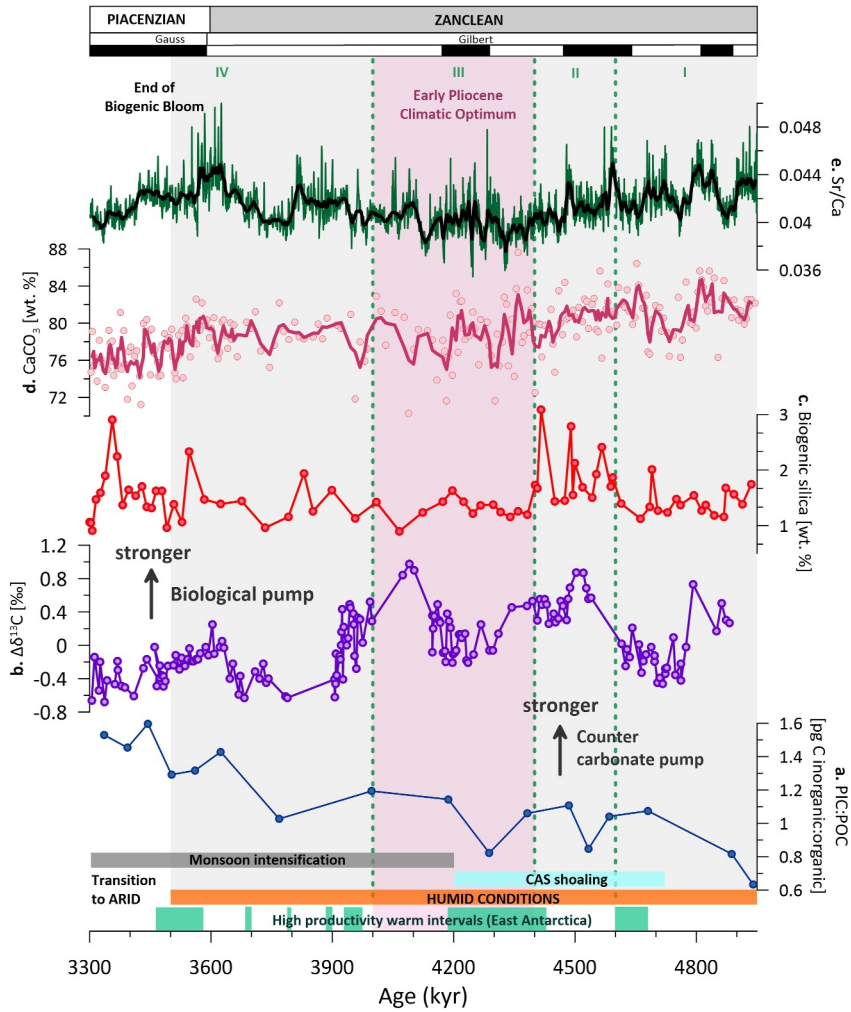

Figure 4. Site U1475 biogeochemical proxies reflecting early Pliocene ocean conditions and the global carbon cycle. (a) Ratio between particulate inorganic and organic carbon (PIC/POC), (b) $\Delta\ \delta^{13}C$ between planktic and benthic foraminifera (*Globigerinoides bulloides - Cibicidoides wuellerstorfi*; ODP Site 114–704) (Hodell & Venz, 1992), biogenic silica (c) wt. % and (d) mass accumulation rate (MAR), biogenic $CaCO_3$ (e) wt. % (raw data: pink circles, three-point running average to highlight the general trend: solid pink line) and (f) MAR, total coccolith (g) absolute abundance and (h) coccolith accumulation rates. Significant paleoceanographic events are indicated: Central American Seaway shoaling (Bell et al., 2015), monsoon intensification (Y. G. Zhang et al., 2009), high productivity warm intervals in East Antarctica (Cook et al., 2013), transition from humid to arid conditions (Christensen et al., 2017), and the later part of the late Miocene to early Pliocene biogenic bloom event (gray bar). Intervals I to IV (green dotted line and text) refer to the intervals discussed in the text.

4.2. Geochemical Proxies

4.2.1. Bulk Calcium Carbonate

Overall $CaCO_3$ content exhibits a decreasing trend, with weight percentages ranging between 87.6% and 65.8% (Figure 4e). The biogenic bloom interval (4.95–3.5 Ma) is characterized by high $CaCO_3$ content, followed by lower values from 3.5 Ma onwards. Notable reductions in $CaCO_3$ content are observed from 4.8 to 4.65 Ma, 4.6 to 4.4 Ma (Interval II), 4.35 to 4.2 Ma, and 4.15 to 4.0 Ma. $CaCO_3$ content remains relatively constant throughout Interval IV, then declines from 3.5 to 3.3 Ma.

4.2.2. Biogenic Silica

The three-step shift observed in coccolithophore assemblages is also evident in the biogenic silica content (Figures 2g and 4c). Biogenic silica is generally low, but slight increases are recorded from 4.95 to 4.6 Ma. Interval II (4.6–4.4 Ma) is characterized by three distinct peaks (up to 3%), which coincide with decreases in *F.*

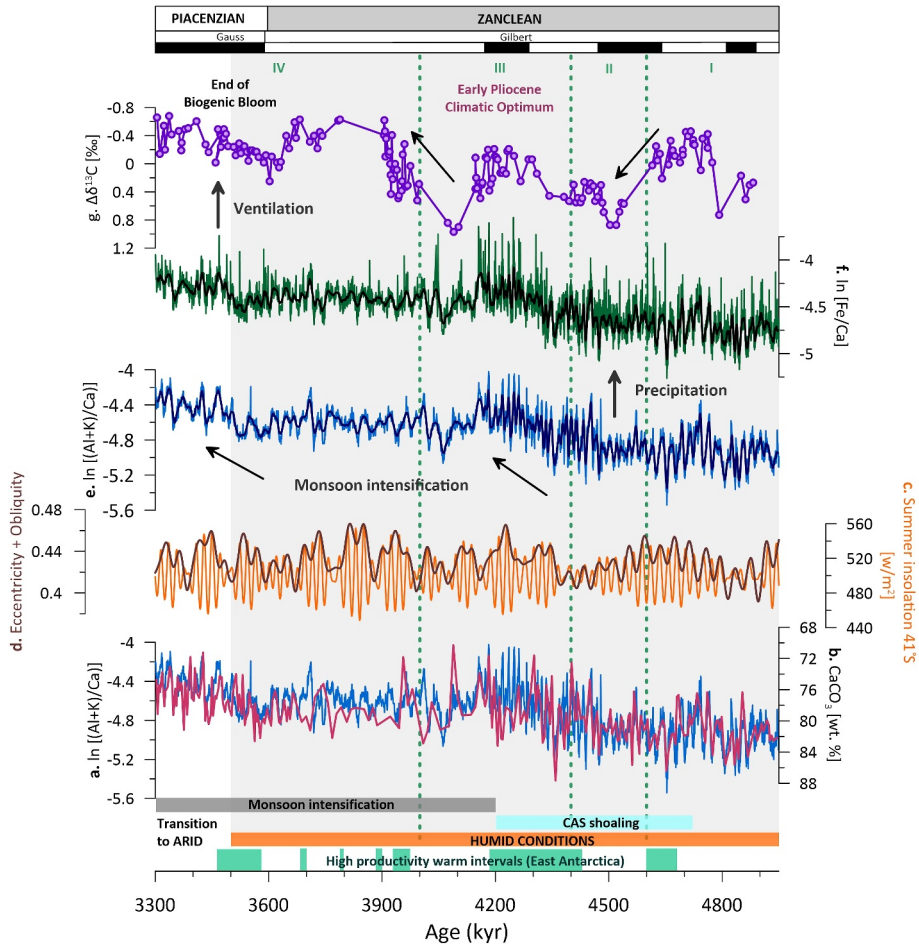

Figure 5. Marine and terrestrial proxy records at Site U1475. (a, e) ln [(Al + K)/Ca)] (X-ray fluorescence (XRF) counts, darker blue solid line is the 19-point running average to highlight long-term trend), (b) $CaCO_3$ wt. %, (c) 21st December insolation (austral summer) at 41˚S (Laskar et al., 2011), (d) eccentricity and obliquity records (Laskar et al., 2011), (f) ln [Fe/Ca)] (XRF counts, black solid line is the 19-point running average to highlight long-term trend), (g) $\Delta\ \delta^{13}C$ between planktic and benthic foraminifera (*Globigerinoides bulloides* - *Cibicidoides wuellerstorfi*; ODP Site 114–704) (Hodell & Venz, 1992). Significant paleoceanographic events are indicated: Central American Seaway shoaling (Bell et al., 2015), monsoon intensification (Y. G. Zhang et al., 2009), high productivity warm intervals in East Antarctica (Cook et al., 2013), transition from humid to arid conditions (Christensen et al., 2017), and the later part of the late Miocene to early Pliocene biogenic bloom event (gray bar). Intervals I to IV (green dotted line and text) refer to the intervals discussed in the text.

profunda abundance and $CaCO_3$ content (Figures 2e and 4e). A steep decline from 3% to 1.5% in biogenic silica content occurred at 4.4 Ma and remained relatively low, but with variable peaks until 3.5 Ma, and increasing toward 3.3 Ma.

4.2.3. XRF-Based Proxies

Fe/Ca ratios are highly variable, displaying a cyclical pattern (Figure 5f). The ln [(Al + K)/Ca)] values demonstrate similar long-term trend with Fe/Ca ratios and opposite with $CaCO_3$ content throughout the record (Figures 5a, 5b, and 5e).

5. Discussion

5.1. Phytoplankton Adaptive Strategies During the Early Pliocene Biogenic Bloom

Paleoclimatic reconstructions underscore the relatively warmer-than-present temperature of several intervals during the Cenozoic (e.g., Zachos et al., 2001). Notable among these climatic events are the Paleocene-Eocene

Thermal Maximum, Miocene Climatic Optimum, and Pliocene warm events (early Pliocene, mid-Pliocene Warm Period). The elevated temperatures during these periods and altered oceanic circulation patterns set the backdrop for a series of biotic responses, leading to the emergence of the so-called biogenic blooms (e.g., Farrell et al., 1995; Karatsolis et al., 2022). These biogenic bloom events, identifiable in geologic records by high accumulation rates of carbonate and biogenic silica (Dickens & Owen, 1999), are characterized by pronounced ecological and climatic shifts in different ocean basins, contributing to alterations in marine biogeochemistry, carbon sequestration, and global climate dynamics.

Around 4.6 Ma, coccolithophore communities in the subtropical Indian Ocean show distinct shifts in assemblage composition and abundance (Figure 2) and morphological characteristics (Figure 3). The observed shift in abundances from larger to smaller *Reticulofenestra* species (Figures 2a and 2b) and Noelaerhabdaceae <5 μm (Figure 2c) reflects the adaptive strategy of this group to environmental change. During this interval, the *Reticulofenestra* communities show prominent morphological adaptations, encompassing changes in cell size and coccolith morphology (Young, 1990). The adaptive strategies employed by coccolithophores, particularly within the *Reticulofenestra* group, offer insights into biological responses to prevailing environmental constraints, such as nutrient availability, SST, and light penetration (Haidar & Thierstein, 2001). In low-latitude regions, a shift in dominance between *Reticulofenestra* to small *Gephyrocapsa* species around 4.42 Ma suggests a shift in ecological preferences (Karatsolis et al., 2022). This change was attributed to species adaptation to warm, stratified conditions, with small *Gephyrocapsa* potentially outcompeting small *Reticulofenestra* in tropical environments. However, the oceanographic conditions at the subtropical Site U1475 may not have favored the proliferation of gephyrocapsids, prompting reticulofenestrids to develop alternative adaptation strategies.

Previous studies have shown that reducing cell volume while increasing abundance is the adaptive mechanism of *Reticulofenestra* to thrive in carbon-limited conditions (Young, 1990). During warm periods of the early Pliocene, reducing cell volume was one of the adapting mechanisms of the *Reticulofenestra* group in the subtropical Indian Ocean, similar to what was observed for the *Gephyrocapsa* group in the North Atlantic and western Mediterranean Sea during the Mid-Bruhnes interval (González-Lanchas et al., 2023). This response was documented during significant paleoclimatic transitions, including the Eocene-Oligocene transition, marked by a substantial decrease in CO_2 levels from >1,000 to <500 ppm (Henderiks & Pagani, 2008). This adaptive trajectory, favoring smaller species such as the smaller size Noelaerhabdaceae with optimized resource acquisition capacities, occurred across all ocean basins over the middle Miocene to Pleistocene epochs, with the transition from a warm and high CO_2 to cold and low CO_2 conditions (Bolton et al., 2016; Hannisdal et al., 2012). The smaller size cells with the higher surface-to-volume ratio have a greater efficiency for resources acquisition relative to cost, favoring the smaller species in carbon-limited oceans during periods of high pCO_2 levels (Bolton et al., 2016). Moreover, warmer, productive environments witnessed significant diversification in coccolith morphogenesis, reflecting variations in coccolith size, thickness, and ornamentation (e.g., Bolton et al., 2016; González-Lanchas et al., 2023; Guitián et al., 2022). Such morphological adaptations facilitated optimized nutrient acquisition and light utilization, thereby conferring competitive advantages within nutrient-rich environments (Brand, 2006; Margalef, 1978).

5.2. The Southern Ocean and the Subtropical Indian Ocean Surface Water Dynamics

The dynamics of surface waters in the Southern Ocean and subtropical Indian Ocean are profoundly influenced by the migration of the STF, a critical boundary separating distinct oceanic regimes: the colder, fresher, nutrient-rich Southern Ocean waters from the south, and the warmer, saltier Agulhas Current waters from the north (Lutjeharms, 2006). Changes in surface water productivity at Site U1475 show a direct response of both calcareous (Flores et al., 1999; Tangunan et al., 2021) and siliceous phytoplankton groups to the STF migration and the Agulhas Current water characteristics (Flores et al., 1999; Romero et al., 2015; Tangunan et al., 2021).

The period between 4.95 and 4.6 Ma exhibited warmer and more stable surface waters (Jatiningrum & Sato, 2017), as evidenced by the high abundances of the larger *Reticulofenestra* (Figures 2a and 2b) and diminished numbers of Noelaerhabdaceae species <5 μm (Figure 2c). Around 4.85 Ma, there was a notable surge in the abundance of the cooler water *C. pelagicus*, suggesting either the expansion of the cold SASW or nutrient enrichment at the site (Figure 2f). The concurrent increase in Noelaerhabdaceae <5 μm points toward nutrient enrichment due to local upwelling or lateral advection of nutrients from the north (Flores et al., 1999), especially since biogenic silica levels at the site remained low (Figure 2g). This signifies that nutrient availability rather than

temperature changes from the entrance of cooler Southern Ocean waters, was the driving force. A strong stratification occurred from 4.85 to 4.8 Ma as evidenced by peak abundances in *F. profunda*, a species known for its affinity to the lower photic layer characterized by limited sunlight (Ahagon et al., 1993; Farida et al., 2012), accompanied by a decline in the upper photic zone group Noelaerhabdaceae <5 μm. This interval also registers two of the highest peaks in total coccolith absolute abundances, primarily comprising *Gephyrocapsa*, *Reticulofenestra*, and *F. profunda*, indicative of a prevailing tropical environment influenced by the Agulhas Current (Flores et al., 1999). Additionally, the abundance of *C. braarudii* from ~4.95 to 4.6 Ma indicates nutrient conditions ranging from mesotrophic to eutrophic (Figure 2f) (Narciso et al., 2006).

A shift indicative of eutrophic conditions and/or enhanced upper ocean mixing is evident after 4.6 Ma, marked by a transition to smaller *Reticulofenestra*, continuing until 3.3 Ma. The increase in biogenic silica from 4.6 to 4.4 Ma (Figure 2g), along with increased abundances of Noelaerhabdaceae species <5 μm corroborates the eutrophic nature of the surface waters (Figure 2c). In contrast, the decline in *F. profunda* abundances suggests more vigorous water column mixing (Figure 2e). The opposite trend between the total coccoliths (Figure 2d) and biogenic silica from 4.6 to 4.4 Ma suggests that the availability of dissolved silica in the water column favored the abundance of diatoms that may have outcompeted the coccolithophores (e.g., Choudhari et al., 2023). This is supported by a reduction in carbonate content, particularly at 4.4 Ma, coinciding with the highest peak in biogenic silica (Figures 4c and 4e), an occurrence documented during Pleistocene glacial periods in the Agulhas Plateau, where carbonates are diluted by high biogenic silica (Romero et al., 2015). During this period, biogenic silica production in the I-AOG, close to the STF, has been associated with the transport of silica-rich intermediate waters from high latitudes to the Agulhas Plateau (Romero et al., 2015). We, therefore, posit that the shift in the dominant phytoplankton group during this interval resulted from the northward expansion of the cold and nutrient-rich SASW. There is a notable increase in the Subantarctic zone biological export production when the STF moves northward, indicative of enhanced nutrient utilization (Martínez-García et al., 2014), alongside elevated fluxes of biogenic detrital components, signifying an increase in the carbon export to the deep ocean (Kohfeld et al., 2005). Following this interpretation, it is plausible that the STF migrated northward between 4.6 and 4.4 Ma, facilitating mixing between the SASW and the Agulhas Current, thereby resulting in increased abundances of smaller *Reticulofenestra*, Noelaerhabdaceae <5 μm, and diatoms. Concurrently, the timing is coincident with the shoaling of the Central American Seaway (Bell et al., 2015), which is likely associated with the restructuring of global nutrient reservoirs, suggesting potential teleconnections between the Pacific and the subtropical Indian Ocean basins during the early Pliocene.

By 4.4 Ma, a decline in biogenic silica marked the onset of the EPCO, indicating the persistent influence of the warm Agulhas Current until 3.6 Ma. The STF is likely positioned further south throughout this interval, with coccolithophores as the main contributors to oceanic primary production. While pulses of increased *C. pelagicus* and biogenic silica are recorded during this time, these levels remain significantly low compared to the previous interval (Figures 2f and 2g). From 3.6 Ma, evidence of surface water cooling is recorded in both biogenic silica and *C. pelagicus*, indicating the mixing of the Agulhas Current waters with SASW at Site U1475, a pattern similar to conditions observed between 4.6 and 4.3 Ma. Additionally, the consistently low abundances of *F. profunda* during this period further suggest the mixing of the upper water column (Figure 2e). Surface water nutrient enrichment, due to increased influence from the Southern Ocean during this interval, increased the abundances of small Noelaerhabdaceae (Figure 2c).

5.3. Progressive Intensification of the Southern African Monsoon From ~4.5 Ma

Detrital clay mineral components of marine sediments reflect continental weathering and erosion, serving as proxies for variations in African, Asian, and South American monsoons (e.g., Colin et al., 2014; Harris & Mix, 2002; Tian et al., 2011). At Site U1475, elemental ratios ln [(Al + K)/Ca] reflect changes in terrestrial input (Figure 5e), similar to observations at Site U1463 located off northwest Australia (Auer et al., 2019), and are used here to infer changes in the intensity of the southern African monsoon. Increased terrestrial input corresponds to heightened precipitation, as stronger monsoon activity leads to more intense rainfall, which in turn enhances weathering and erosion on the continent.

Comparing precipitation variability with both carbonate and total coccolith absolute abundance records reveals a robust inverse correlation between ln [(Al + K)/Ca] and bulk $CaCO_3$ ($R = -0.70$; Figure 5a, Figure S2 in Supporting Information S1) and a weaker negative correlation with total coccolith CARs ($R = -0.31$; Figure S2 in

Supporting Information S1). This suggests that terrigenous sediment supply predominantly controls surface water carbonate production and its consequent deposition and preservation at the site. However, it is important to consider the potential influence of dilution or concentration effects, where fluctuations in carbonate productivity may affect the concentration of terrestrial sediments. Despite similarities in long-term trend between ln [(Al + K)/Ca] and ln Fe/Ca (Figures 5e and 5f), poor correlation is recorded ($R = 0.20$; Figure S2 in Supporting Information S1) at the Agulhas Plateau suggesting that these elemental ratios are influenced by different processes or sources in this region at shorter timescales (Caley et al., 2018).

Sediment materials at the Agulhas Plateau consist of nannofossil ooze, alternating between foraminifer-bearing or foraminifer-rich nannofossil ooze and nannofossil ooze with fine sand (foraminifer, quartz, and occasionally diatoms) (Hall et al., 2017b). This would suggest that planktic organisms such as coccolithophores are the main contributors to carbonate production at U1475. However, the poor correlation between total coccolith abundance and bulk $CaCO_3$ ($R = 0.24$; Figure S2 in Supporting Information S1), suggests other sources of $CaCO_3$ in the water column and the seafloor, such as planktic foraminifer and pteropods (Bramlette, 1958) or carbonates that are eroded (Alonso-Garcia et al., 2024) and transported from the South African shelf by the Agulhas Current.

The latest Miocene biogenic bloom is characterized by an enhanced delivery of dissolved nutrients into the oceans (Dickens & Owen, 1999), coinciding with the onset of Indian monsoons between 7 and 6 Ma (Molnar et al., 2010). During the early Pliocene, southern African monsoon intensification at Site U1475 is evidenced by increase in detrital input, which is primarily composed of terrigenous components originating from the African continent (Caley et al., 2018). This detrital input serves as a proxy for the terrestrial material washed into the ocean through increased runoff during periods of heightened monsoon activity. As a result of this increased terrigenous input, there is a subsequent reduction in carbonate deposition at the site. However, it is crucial to consider the potential influence of changes in the transport regime, such as the strengthening of the Agulhas Current or variations in bottom water flow. Given that Site U1475 is located on a drift site (Gruetzner et al., 2019), these changes in ocean dynamics could affect the transportation and distribution of terrigenous material, ultimately impacting the observed detrital input and its relationship with monsoon intensity.

Periods of intensified monsoon activity can result in enhanced rainfall over the South African region (e.g., Taylor et al., 2021) leading to increased runoff and freshwater input into the surrounding ocean. Records of ln [(Al + K)/Ca] and ln (Fe/Ca) ratios suggest a weaker monsoon intensity from 4.95 to ∼4.5 Ma, followed by a subsequent intensification from ∼4.5 to 4.2 Ma at the beginning of the EPCO, continuing until 3.3 Ma. The ln (Fe/Ca) ratio shows heightened terrestrial input around 4.5 Ma, corresponding to the intensification of the southern African monsoon (Figure 5f). This period of increased precipitation is further supported by the ln [(Al + K)/Ca] ratio (Auer et al., 2019), which peaks around 4.5 Ma, reflecting stronger monsoon activity (Figure 5e). The overall increase in ln [(Al + K/Ca)] and ln (Fe/Ca) is supported by an increase in Noelaerhabdaceae and a decline in *F. profunda* suggesting a long-term increase in regional precipitation. Notably, this intensification onset of the southern African monsoon precedes the recorded strengthening of the Asian monsoon at 4.2 Ma (Y. G. Zhang et al., 2009), highlighting potential hemispheric climate linkages and the need to understand their relative contributions to global climate dynamics. Orbital forcing, as indicated by eccentricity and obliquity cycles, aligns with these climatic variations, particularly from 4.5 to 3.9 Ma. Peaks in summer insolation at the location (41°S) around 4.2, 3.8, and 3.4 Ma also correlate with increased monsoon intensity and precipitation, indicating the influence of solar radiation on regional climate (Figures 5c and 5d).

In the Benguela upwelling region, the southern African monsoon significantly influences the strength of the southeast trade winds, which facilitate water column mixing and subsequently enhance productivity during the biogenic bloom (Diester-Haass et al., 2005). These prevailing wind systems, including the trade winds and westerlies, have shifted in the past and are forecasted to move poleward (Tim et al., 2019). Such shifts could impact the Agulhas Current system and directly alter precipitation patterns in the southern African region (Tim et al., 2023).

Strong precipitation can lead to enhanced chemical weathering (Filippelli, 1997; Tian et al., 2011), resulting in increased terrestrial input to the oceans and subsequently boosting nutrient delivery (L. Zhang et al., 2009), potentially fueling the increased production of carbonate and siliceous organisms from ∼4.5 to 3.3 Ma. However, the availability of dissolved silica in the water column may have favored the proliferation of diatoms over the Agulhas Plateau, potentially outcompeting coccolithophores. During this period, the decline in the recorded total coccolith abundance at the site resulted from decreased coccolithophore productivity is likely due to competition,

dilution by biogenic silica (Romero et al., 2015), dilution by freshwater due to increased precipitation, and dissolution (Gottschalk et al., 2018).

The evolution of spectral characteristics of the Site U1475 proxies identifies the main astronomical drivers controlling the southern African monsoon. The ln[(Al + K)/Ca] ratio, representing terrestrial precipitation, follows a pattern with initial long-period cycles at ~400 kyr transitioning to shorter cycles of precession (23.8 kyr) and semi-precession (16.6 kyr) (Figure 6c). Similarly, the spectral power density plot of Fe/Ca identifies prominent periodicities at 100, 23.8, and 19.2 kyr (Figure 6d). This response of terrestrial records to precession indicates that local insolation forcing (Figures 5c, 6c, and 6d) controlled the strengths of atmospheric circulation and precipitation in the Indian sector of the Southern Ocean. A cross-spectral analysis between precession and terrestrial precipitation record between 4.95 and 4.5 Ma revealed a lag of approximately 3–5 kyr between precession maxima and precipitation maxima, suggesting a delayed climatic response to insolation changes (Figure S3 in Supporting Information S1). This lag points to the complexity of Earth's climate system, where internal feedback and ocean-atmosphere interactions might contribute to the temporal offset. Around 4.5 Ma and 3.9 Ma, all four proxies exhibit notable shifts in power frequency, marked by transitions from longer to shorter periodicities. These shifts, visible in the spectral power plots, highlight a change in the dominant climatic forces affecting the Agulhas Plateau. Starting around 4.95 Ma, *F. profunda*, an indicator of water column stratification, shows dominant long eccentricity cycles (~400 kyr), indicating stable, long-period stratification dynamics (Figure 6a). Shorter eccentricity cycles (~100 kyr) occurred afterwards, suggesting increased variability in stratification. Concurrently, $CaCO_3$, reflecting changes in productivity and carbonate preservation, displays significant peaks at ~100 kyr, with additional shorter cycles, indicating a shift towards more frequent climatic fluctuations (Figure 6b). This reflects a complex interplay between Earth's orbital parameters and regional climatic conditions, influencing stratification, carbonate dynamics, and terrestrial precipitation, culminating in increased climatic variability by 3.3 Ma.

5.4. Implications for the Carbonate Pump and Global Climate

The interplay between variability in surface and deep ocean currents and biological assemblages holds significant implications for global biogeochemical cycles and, consequently, overarching climate dynamics. Atmospheric CO_2 is considered an essential driver of coccolithophore evolution during the Cenozoic (Bolton et al., 2016; Henderiks & Pagani, 2008). These organisms are integral to the carbonate pump, a mechanism fundamental for modulating pCO_2 concentrations by facilitating the export of carbonates from the surface ocean to the deep sea, and the effect of change in carbon ballasting on the BCP efficiency (Klaas & Archer, 2002). The significance of the BCP in the global climate system can be attributed, in large part, to the net flux of CO_2 into or out of the atmosphere (Sigman & Boyle, 2000), which is controlled by primary production in the surface. In response to fluctuating CO_2 regimes, it is postulated that coccolithophores evolved sophisticated Carbon Concentrating Mechanisms to augment their photosynthetic efficiency, particularly within nutrient-rich environments (Rost & Riebesell, 2004). Previous studies suggested that these mechanisms facilitated an accelerated rate of CO_2 fixation, thereby promoting cellular growth and reproductive success during this period (e.g., Badger, 2021; Rost & Riebesell, 2004).

Within the mesotrophic subtropical region of the Southern Ocean, where coccolithophores are in high concentrations, biological productivity is a key component of the ocean's carbon pump (Flores et al., 1999). Carbon dioxide exchange between the ocean and atmosphere in the Southern Ocean is exceptionally high, where deep waters enriched in respired CO_2 and nutrients are brought to the surface by vertical mixing (e.g., upwelling) (Arrigo et al., 1999), promoting high rates of phytoplankton productivity in the photic layer (Jaccard et al., 2013). Increased rates in vertical mixing shown by lower $\Delta\ \delta^{13}C$ (*Globigerinoides bulloides* - *Cibicidoides wuellerstorfi*) from ODP 704 in the South Atlantic (Hodell & Venz, 1992) during the early Pliocene (Figure 4b) are coincident with high abundances of the upper photic zone group Noelaerhabdaceae (mostly *Reticulofenestra*) with affinity for meso-to eutrophic conditions, and high abundances of biogenic silica at Site U1475 (Figures 2a, 2d, and 2g), suggesting that ocean circulation changes directly modulate surface water production at the Agulhas Plateau. This is similar to the Pleistocene coccolith record within the Agulhas region, which was influenced by a strong vertical mixing (Flores et al., 1999).

From 4 Ma, $CaCO_3$ and coccolith records indicate a switch in primary producers, with diatoms outcompeting coccolithophores. This further implies that the inferred change in productivity reflects the phytoplankton response

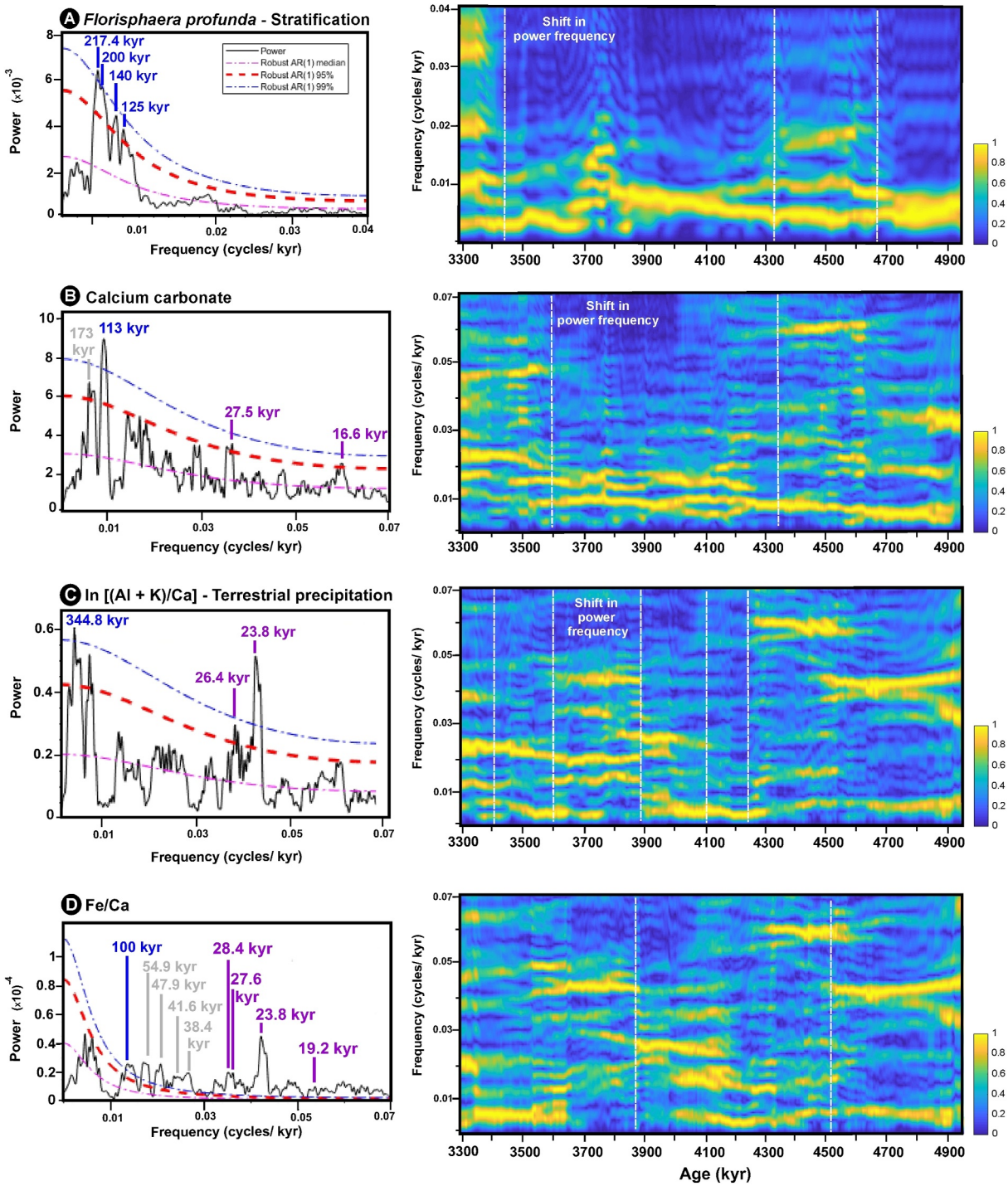

Figure 6. Power spectral density (left panels) and wavelet power spectra (right panels) for various marine and terrestrial proxies at Site U1475 during the early Pliocene, showing shifts in dominant periodicities and their evolution over time. (a) *Florisphaera profunda* as an indicator of water column stratification, (b) Bulk calcium carbonate wt. %, (c) ln [(Al + K)/Ca] as a proxy for terrestrial precipitation, (d) Fe/Ca as a proxy for detrital input. Each left panel displays significant periodicities in the power spectrum, indicated by the black, blue, and red lines corresponding to the Robust AR1 1 median, 95%, and 99% significance levels, respectively. Right panels show the wavelet power spectra, with color intensity representing power strength and significant periodicities outlined by the dashed lines. Notable shifts in power frequency are highlighted, indicating changes in climatic and oceanographic conditions over time.

to nutrient enrichment via ocean circulation and nutrient supply both from deeper waters and from lateral advection of nutrients from the south of the study area. While intensified vertical mixing enhances phytoplankton proliferation, it compromises the efficacy of the BCP. By elevating nutrient concentrations with the surface waters, mixing promotes phytoplankton blooms but attenuates the efficiency of the BCP in sequestering pCO_2. This is corroborated by carbonate content at Site U1475, showing a diminishing trend, with shifts during the EPCO (4.4 Ma) and at 3.6 Ma (Figure 4d), coinciding with changes in Southern Ocean ventilation but showing an opposite trend (Figure 4b). This intensified ocean circulation and mixing, particularly between 4.0 and 3.5 Ma (Hodell & Venz, 1992; Hodell & Warnke, 1991), led to increased phytoplankton production, disrupting the efficiency of the BCP (e.g., Duchamp-Alphonse et al., 2018; Villa et al., 2014). As phytoplankton proliferated, they absorbed more CO_2 from the atmosphere (via photosynthesis), but the subsequent sinking of organic matter to the deep ocean was slowed down by enhanced mixing, preventing efficient sequestration of carbon in the deep ocean. This disruption in the BCP resulted in reduced carbon storage in the deep ocean, potentially contributing to elevated pCO_2 levels and acting as a precursor to the subsequent prolonged warmth of the MPWP.

6. Conclusions

Our study provides insights into the early Pliocene "biogenic bloom" in the southwestern Indian Ocean, emphasizing the combined influence of both the Southern Ocean and the southern African monsoon variability in driving changes in BCP. Phytoplankton adaptive strategies, particularly within the *Reticulofenestra* group, reveal responses to changing environmental conditions, including cell size and morphological alterations. Surface water dynamics, influenced by the STF migration, the Agulhas Current, and the SASW, modulate phytoplankton productivity and community structure, with transitions to cooler, nutrient-enriched conditions coinciding with shifts in phytoplankton assemblage composition.

The progressive intensification of the southern African monsoon from ∼4.5 Ma, evidenced by increased terrigenous input, precedes the strengthening of the Asian monsoon estimated at ∼4.2 Ma, and highlights the complex interplay between regional climate systems. These findings have implications for global biogeochemical cycles, particularly the efficacy of the global carbonate pump, and underscore the sensitivity of marine ecosystems to environmental changes. Therefore, investigating the Indian sector of the Southern Ocean is crucial as future changes in the Agulhas Current system could impact precipitation patterns across southern Africa. Understanding the dynamics of the Agulhas Current system and the Southern Ocean is essential for predicting and adapting to potential shifts in regional and global climate patterns in the coming decades.

Data Availability Statement

This research used samples provided by the IODP. All new data sets are archived on Zenodo. Calcareous nannofossil assemblage relative abundances and coccolith morphometry are available as Tangunan, Flores, and LeVay (2024), https://doi.org/10.5281/zenodo.14291181 and Tangunan, Flores, and Fuertes (2024), https://doi.org/10.5281/zenodo.14291319, respectively. The sediment elemental XRF data set is available as Hall et al. (2024), https://doi.org/10.5281/zenodo.14291349. The bulk calcium carbonate record is available as LeVay (2024), https://doi.org/10.5281/zenodo.14291394. The biogenic silica data set is available as Coenen (2024), https://doi.org/10.5281/zenodo.14341433.

Acknowledgments
This work used sediments and data provided by the IODP. We are thankful for the support from the R/V JOIDES Resolution crew and IODP staff. We thank the two reviewers for their constructive feedback and the Associate Editor and Editor Ursula Röhl for their careful handling of the manuscript. This work was funded through the Universidad de Salamanca Postdoctoral Contract awarded to D.N.T., supported by the Ministerio de Ciencia, Innovación y Universidades Grant RTI2018-099489-B-I00. We also acknowledge funding support from the European Union's Horizon 2020 Research and Innovation Programme under the Marie Sklodowska Curie Grant Agreement No. 885498 and the European Consortium for Ocean Research Drilling Research Grant. J.J.C. acknowledges USSSP Post Expedition Award and Geological Society of America Graduate student research grant.

References

Acker, J. G., & Leptoukh, G. (2007). Online analysis enhances use of NASA earth science data. *Eos, Transactions American Geophysical Union*, *88*(2), 14–17. https://doi.org/10.1029/2007eo020003

Ahagon, N., Tanaka, Y., & Ujiie, H. (1993). Florisphaera profunda, a possible nannoplankton indicator of late Quaternary changes in sea-water turbidity at the northwestern margin of the Pacific, Mar Micropaleontol (pp. 255–273).

Ahn, S., Khider, D., Lisiecki, L. E., & Lawrence, C. E. (2017). A probabilistic Pliocene–Pleistocene stack of benthic δ18O using a profile hidden Markov model. *Dynamics and Statistics of the Climate System*, *2*(1). https://doi.org/10.1093/climsys/dzx002

Alonso-Garcia, M., Reolid, J., Jimenez-Espejo, F. J., Bialik, O. M., Alvarez Zarikian, C. A., Laya, J. C., et al. (2024). Sea-level and monsoonal control on the Maldives carbonate platform (Indian Ocean) over the last 1.3 million years. *Climate of the Past*, *20*(3), 547–571. https://doi.org/10.5194/cp-20-547-2024

Arrigo, K. R., Robinson, D. H., Worthen, D. L., Dunbar, R. B., DiTullio, G. R., VanWoert, M., & Lizotte, M. P. (1999). Phytoplankton community structure and the drawdown of nutrients and CO2 in the southern ocean. *Science*, *283*(5400), 365–367. https://doi.org/10.1126/science.283.5400.365

Auer, G., De Vleeschouwer, D., Smith, R. A., Bogus, K., Groeneveld, J., Grunert, P., et al. (2019). Timing and pacing of Indonesian throughflow restriction and its connection to late Pliocene climate shifts. *Paleoceanography and Paleoclimatology*, *34*(4), 635–657. https://doi.org/10.1029/2018pa003512

Backman, J., & Hermelin, J. O. R. (1986). Morphometry of the Eocene nannofossil Reticulofenestra umbilicus lineage and its biochronological consequences. *Palaeogeography, Palaeoclimatology, Palaeoecology*, *57*(1), 103–116. https://doi.org/10.1016/0031-0182(86)90009-x

Badger, M. P. S. (2021). Alkenone isotopes show evidence of active carbon concentrating mechanisms in coccolithophores as aqueous carbon dioxide concentrations fall below 7 μmol L^{-1}. *Biogeosciences*, *18*(3), 1149–1160. https://doi.org/10.5194/bg-18-1149-2021

Balch, W., Drapeau, D., Bowler, B., & Booth, E. (2007). Prediction of pelagic calcification rates using satellite measurements. *Deep Sea Research Part II: Topical Studies in Oceanography*, *54*(5–7), 478–495. %@ 0967-0645. https://doi.org/10.1016/j.dsr2.2006.12.006

Balch, W. M., Bates, N. R., Lam, P. J., Twining, B. S., Rosengard, S. Z., Bowler, B. C., et al. (2016). Factors regulating the Great Calcite Belt in the Southern Ocean and its biogeochemical significance. *Global Biogeochemical Cycles*, *30*(8), 1124–1144. https://doi.org/10.1002/2016gb005414

Bartoli, G., Hönisch, B., & Zeebe, R. E. (2011). Atmospheric CO2 decline during the Pliocene intensification of Northern Hemisphere glaciations. *Paleoceanography*, *26*(4). https://doi.org/10.1029/2010pa002055

Beal, L. M., Ruijter, W. P. M. D., Biastoch, A., Zahn, R., Cronin, M., Hermes, J., et al. (2011). On the role of the Agulhas system in ocean circulation and climate. *Nature*, *472*(7344), 429–436. https://doi.org/10.1038/nature09983

Bell, D. B., Jung, S. J., Kroon, D., Hodell, D. A., Lourens, L. J., & Raymo, M. E. (2015). Atlantic deep-water response to the early Pliocene shoaling of the Central American Seaway. *Scientific Reports*, *5*(1), 12252. https://doi.org/10.1038/srep12252

Biastoch, A., Böning, C. W., Schwarzkopf, F. U., & Lutjeharms, J. (2009). Increase in Agulhas leakage due to poleward shift of Southern Hemisphere westerlies. *Nature*, *462*(7272), 495–498. https://doi.org/10.1038/nature08519

Bolton, C. T., Hernandez-Sanchez, M. T., Fuertes, M. A., Gonzalez-Lemos, S., Abrevaya, L., Mendez-Vicente, A., et al. (2016). Decrease in coccolithophore calcification and CO2 since the middle Miocene. *Nature Communications*, *7*(1), 10284. https://doi.org/10.1038/ncomms10284

Bramlette, M. (1958). Significance of coccolithophorids in calcium-carbonate deposition. *Geological Society of America Bulletin*, *69*(1), 121–126. https://doi.org/10.1130/0016-7606(1958)69[121:socicd]2.0.co;2

Brand, L. (2006). Physiological ecology of marine. *Coccolithophores*, *39*.

Brandon, M., Duchamp-Alphonse, S., Michel, E., Landais, A., Isguder, G., Richard, P., et al. (2022). Enhanced Carbonate Counter Pump and upwelling strengths in the Indian sector of the Southern Ocean during MIS 11. *Quaternary Science Reviews*, *287*, 107556. https://doi.org/10.1016/j.quascirev.2022.107556

Brierley, C. M., & Fedorov, A. V. (2016). Comparing the impacts of Miocene–Pliocene changes in inter-ocean gateways on climate: Central American Seaway, Bering Strait, and Indonesia. *Earth and Planetary Science Letters*, *444*, 116–130. https://doi.org/10.1016/j.epsl.2016.03.010

Brierley, C. M., Fedorov, A. V., Liu, Z., Herbert, T. D., Lawrence, K. T., & Lariviere, J. P. (2009). Greatly expanded tropical warm pool and weakened Hadley circulation in the early Pliocene. *Science*, *323*(5922), 1714–1718. https://doi.org/10.1126/science.1167625

Caley, T., Extier, T., Collins, J. A., Schefuss, E., Dupont, L., Malaize, B., et al. (2018). A two-million-year-long hydroclimatic context for hominin evolution in southeastern Africa. *Nature*, *560*(7716), 76–79. https://doi.org/10.1038/s41586-018-0309-6

Cartagena-Sierra, A., Berke, M. A., Robinson, R. S., Marcks, B., Castañeda, I. S., Starr, A., et al. (2021). Latitudinal migrations of the subtropical front at the Agulhas Plateau through the mid-pleistocene transition. *Paleoceanography and Paleoclimatology*, *36*(7). https://doi.org/10.1029/2020pa004084

Choudhari, P., Nair, A., Mohan, R., & Patil, S. (2023). Variations in the Southern Ocean carbonate production, preservation, and hydrography for the past 41, 500 years: Evidence from coccolith and CaCO3 records. *Palaeogeography, Palaeoclimatology, Palaeoecology*, *614*, 111425. https://doi.org/10.1016/j.palaeo.2023.111425

Christensen, B. A., Renema, W., Henderiks, J., De Vleeschouwer, D., Groeneveld, J., Castañeda, I. S., et al. (2017). Indonesian Throughflow drove Australian climate from humid Pliocene to arid Pleistocene. *Geophysical Research Letters*, *44*(13), 6914–6925. https://doi.org/10.1002/2017gl072977

Clark, C. O., Webster, P. J., & Cole, J. E. (2003). Interdecadal variability of the relationship between the Indian Ocean zonal mode and East African coastal rainfall anomalies. *Journal of Climate*, *16*(3), 548–554. https://doi.org/10.1175/1520-0442(2003)016<0548:ivotrb>2.0.co;2

Cleveland, W. S. (1979). Robust locally weighted regression and smoothing scatterplots. *Journal of the American Statistical Association*, *74*(368), 829–836. %@ 0162-1459. https://doi.org/10.2307/2286407

Clift, P. D., Betzler, C., Clemens, S. C., Christensen, B., Eberli, G. P., France-Lanord, C., et al. (2022). A synthesis of monsoon exploration in the Asian marginal seas. *Scientific Drilling*, *31*, 1–29. https://doi.org/10.5194/sd-31-1-2022

Coenen, J. (2024). Biogenic silica at IODP site U1475 during the early Pliocene [Dataset]. *Zenodo*. https://zenodo.org/records/14341433

Colin, C., Siani, G., Liu, Z., Blamart, D., Skonieczny, C., Zhao, Y., et al. (2014). Late Miocene to early Pliocene climate variability off NW Africa (ODP Site 659). *Palaeogeography, Palaeoclimatology, Palaeoecology*, *401*, 81–95. https://doi.org/10.1016/j.palaeo.2014.02.015

Cook, C. P., van de Flierdt, T., Williams, T., Hemming, S. R., Iwai, M., Kobayashi, M., et al. (2013). Dynamic behaviour of the East Antarctic ice sheet during Pliocene warmth. *Nature Geoscience*, *6*(9), 765–769. https://doi.org/10.1038/ngeo1889

De Boer, A. M., Graham, R. M., Thomas, M. D., & Kohfeld, K. E. (2013). The control of the Southern Hemisphere Westerlies on the position of the Subtropical Front. *Journal of Geophysical Research: Oceans*, *118*(10), 5669–5675. https://doi.org/10.1002/jgrc.20407

Dickens, G. R., & Owen, R. M. (1999). The latest Miocene–early Pliocene biogenic bloom: A revised Indian Ocean perspective. *Marine Geology*, *161*(1), 75–91. https://doi.org/10.1016/s0025-3227(99)00057-2

Dickson, A. J., Leng, M. J., Maslin, M. A., & Röhl, U. (2010). Oceanic, atmospheric and ice-sheet forcing of South East Atlantic Ocean productivity and South African monsoon intensity during MIS-12 to 10. *Quaternary Science Reviews*, *29*(27–28), 3936–3947. https://doi.org/10.1016/j.quascirev.2010.09.014

Diester-Haass, L., Billups, K., & Emeis, K. C. (2005). In search of the late Miocene–early Pliocene "biogenic bloom" in the Atlantic Ocean (Ocean Drilling Program Sites 982, 925, and 1088). *Paleoceanography*, *20*(4). https://doi.org/10.1029/2005pa001139

Diester-Haass, L., Meyers, P. A., & Bickert, T. (2004). Carbonate crash and biogenic bloom in the late Miocene: Evidence from ODP Sites 1085, 1086, and 1087 in the Cape Basin, southeast Atlantic Ocean. *Paleoceanography*, *19*(1). https://doi.org/10.1029/2003pa000933

Dowsett, H. J., Foley, K. M., Stoll, D. K., Chandler, M. A., Sohl, L. E., Bentsen, M., et al. (2013). Sea surface temperature of the mid-Piacenzian ocean: A data-model comparison. *Scientific Reports*, *3*(1), 2013. https://doi.org/10.1038/srep02013

Duchamp-Alphonse, S., Siani, G., Michel, E., Beaufort, L., Gally, Y., & Jaccard, S. L. (2018). Enhanced ocean-atmosphere carbon partitioning via the carbonate counter pump during the last deglacial. *Nature Communications*, *9*, 1–10. %@ 2041-1723. https://doi.org/10.1038/s41467-018-04625-7

Dutton, A., Carlson, A. E., Long, A. J., Milne, G. A., Clark, P. U., DeConto, R., et al. (2015). Sea-level rise due to polar ice-sheet mass loss during past warm periods. *Science*, *349*(6244), aaa4019. https://doi.org/10.1126/science.aaa4019

Farida, M., Imai, R., & Sato, T. (2012). Miocene to Pliocene paleoceanography of the western equatorial Pacific Ocean based on calcareous nannofossils, ODP Hole 805B. *Open Journal of Geology*, *02*, 72–79. https://doi.org/10.4236/ojg.2012.22008

Farrell, J. W., Raffi, I., Janecek, T. R., Murray, D. W., Levitan, M., Dadey, K. A., et al. (1995). 35. Late Neogene sedimentation patterns in the eastern equatorial Pacific. *Ocean*, 2419–2426.

Fedorov, A. V., Brierley, C. M., Lawrence, K. T., Liu, Z., Dekens, P. S., & Ravelo, A. C. (2013). Patterns and mechanisms of early Pliocene warmth. *Nature*, *496*(7443), 43–49. https://doi.org/10.1038/nature12003

Filippelli, G. M. (1997). Intensification of the Asian monsoon and a chemical weathering event in the late Miocene–early Pliocene: Implications for late Neogene climate change. *Geology*, *25*(1), 27. https://doi.org/10.1130/0091-7613(1997)025<0027:iotama>2.3.co;2

Filippelli, G. M., & Flores, J.-A. (2009). From the warm Pliocene to the cold Pleistocene: A tale of two oceans. *Geology*, *37*(10), 959–960. https://doi.org/10.1130/focus102009.1

Flores, J.-A., Gersonde, R., & Sierro, F. J. (1999). Pleistocene fluctuations in the Agulhas Current Retroflection based on the calcareous plankton record. *Marine Micropaleontology*, *37*, 1–22. https://doi.org/10.1016/s0377-8398(99)00012-2

Flores, J. A., & Sierro, F. J. (1997). Revised technique for calculation of calcareous nannofossil accumulation rates. *Micropaleontology*, *43*(3), 321–324. %@ 0026-2803. https://doi.org/10.2307/1485832

Fuertes, M.-Á., Flores, J.-A., & Sierro, F. J. (2014). The use of circularly polarized light for biometry, identification and estimation of mass of coccoliths. *Marine Micropaleontology*, *113*, 44–55. https://doi.org/10.1016/j.marmicro.2014.08.007

Gebregiorgis, D., Giosan, L., Hathorne, E. C., Anand, P., Nilsson-Kerr, K., Plass, A., et al. (2020). What can we learn from X-ray fluorescence core scanning data? A paleomonsoon case study. *Geochemistry, Geophysics, Geosystems*, *21*(2). https://doi.org/10.1029/2019gc008414

Gibbs, S. J., Young, J. R., Bralower, T. J., & Shackleton, N. J. (2005). Nannofossil evolutionary events in the mid-Pliocene: An assessment of the degree of synchrony in the extinctions of Reticulofenestra pseudoumbilicus and Sphenolithus abies. *Palaeogeography, Palaeoclimatology, Palaeoecology*, *217*(1–2), 155–172. https://doi.org/10.1016/j.palaeo.2004.11.005

González-Lanchas, A., Rickaby, R. E. M., Sierro, F. J., Rigual-Hernández, A. S., Alonso-García, M., & Flores, J. A. (2023). Globally enhanced calcification across the coccolithophore Gephyrocapsa complex during the mid-Brunhes interval. *Quaternary Science Reviews*, *321*, 108375. https://doi.org/10.1016/j.quascirev.2023.108375

Gottschalk, J., Hodell, D. A., Skinner, L. C., Crowhurst, S. J., Jaccard, S. L., & Charles, C. (2018). Past carbonate preservation events in the deep southeast Atlantic Ocean (Cape Basin) and their implications for Atlantic overturning dynamics and marine carbon cycling. *Paleoceanography and Paleoclimatology*, *33*(6), 643–663. https://doi.org/10.1029/2018pa003353

Gregg, W. W., & Rousseaux, C. S. (2014). Decadal trends in global pelagic ocean chlorophyll: A new assessment integrating multiple satellites, in situ data, and models. *Journal of Geophysical Research: Oceans*, *119*(9), 5921–5933. https://doi.org/10.1002/2014jc010158

Gruetzner, J., Jiménez Espejo, F. J., Lathika, N., Uenzelmann-Neben, G., Hall, I. R., Hemming, S. R., & LeVay, L. J. (2019). A new seismic stratigraphy in the Indian-Atlantic Ocean Gateway resembles major paleo-oceanographic changes of the last 7 Ma. *Geochemistry, Geophysics, Geosystems*, *20*(1), 339–358. https://doi.org/10.1029/2018gc007668

Guitián, J., Fuertes, M. Á., Flores, J.-A., Hernández-Almeida, I., & Stoll, H. (2022). Variation in calcification of Reticulofenestra coccoliths over the Oligocene–Early Miocene. *Biogeosciences*, *19*(20), 5007–5019. https://doi.org/10.5194/bg-19-5007-2022

Haidar, A. T., & Thierstein, H. R. (2001). Coccolithophore dynamics off Bermuda (N. Atlantic). *Deep Sea Research Part II: Topical Studies in Oceanography*, *48*(8–9), 1925–1956. %@ 0967-0645. https://doi.org/10.1016/s0967-0645(00)00169-7

Hall, I., LeVay, L. J., Berke, M., Coenen, J., Gruetzner, J., Jimenez-Espejo, F. J., & Tangunan, D. (2024). Sediment elemental X-ray fluorescence record at IODP Site U1475 during the early Pliocene [Dataset]. *Zenodo*. Retrieved from https://zenodo.org/records/14291349

Hall, I. R., Hemming, S. R., LeVay, L. J., Barker, S., Berke, M. A., Brentegani, L., et al. (2017a). Expedition 361 methods. In I. R. Hall, S. R. Hemming, L. J. LeVay, & the Expedition 361 Scientists (Eds.), *South African climates (Agulhas LGM density profile)*. International Ocean Discovery Program.

Hall, I. R., Hemming, S. R., LeVay, L. J., Barker, S., Berke, M. A., Brentegani, L., et al. (2017b). Site U1475. In I. R. Hall, S. R. Hemming, L. J. LeVay, & The Expedition 361 Scientists (Eds.), *South African climates (Agulhas LGM density profile)*. International Ocean Discovery Program.

Hannisdal, B., Henderiks, J., & Liow, L. H. (2012). Long-term evolutionary and ecological responses of calcifying phytoplankton to changes in atmospheric CO_2. *Global Change Biology*, *18*(12), 3504–3516. https://doi.org/10.1111/gcb.12007

Harris, S. E., & Mix, A. C. (2002). Climate and tectonic influences on continental erosion of tropical South America, 0–13 Ma. *Geology*, *30*(5), 447. https://doi.org/10.1130/0091-7613(2002)030<0447:catioc>2.0.co;2

Hay, W. W. (2004). *Carbonate fluxes and calcareous nannoplankton* (pp. 509–528). Coccolithophores. Springer.

Henderiks, J., & Pagani, M. (2008). Coccolithophore cell size and the Paleogene decline in atmospheric CO_2. *Earth and Planetary Science Letters*, *269*(3–4), 576–584. https://doi.org/10.1016/j.epsl.2008.03.016

Hermoyian, C. S., & Owen, R. M. (2001). Late Miocene-early Pliocene biogenic bloom: Evidence from low-productivity regions of the Indian and Atlantic Oceans. *Paleoceanography*, *16*(1), 95–100. https://doi.org/10.1029/2000pa000501

Hodell, D. A., & Venz, K. (1992). Toward a high-resolution stable isotopic record of the Southern Ocean during the Pliocene-Pleistocene (4.8 to 0.8 MA). In J. P. Kennett & D. A. Warkne (Eds.), *The Antarctic paleoenvironment: A perspective on global change: Part One* (pp. 265–310).

Hodell, D. A., & Warnke, D. A. (1991). Climatic evolution of the Southern Ocean during the Pliocene epoch from 4.8 to 2.6 million years ago. *Quaternary Science Reviews*, *10*(2–3), 205–214. %@ 0277-3791. https://doi.org/10.1016/0277-3791(91)90019-q

Holliday, N. P., & Read, J. F. (1998). Surface oceanic fronts between Africa and Antarctica. *Deep Sea Research Part I: Oceanographic Research Papers*, *45*(2–3), 217–238. https://doi.org/10.1016/s0967-0637(97)00081-2

Jaccard, S. L., Hayes, C. T., Martinez-Garcia, A., Hodell, D. A., Anderson, R. F., Sigman, D. M., & Haug, G. H. (2013). Two modes of change in Southern Ocean productivity over the past million years. *Science*, *339*(6126), 1419–1423. https://doi.org/10.1126/science.1227545

Jatiningrum, R. S., & Sato, T. (2017). Sea-surface dynamics changes in the subpolar North Atlantic Ocean (IODP site U1314) during late Pliocene climate transition based on calcareous nannofossil observation. *Open Journal of Geology*, *07*(10), 1538–1551. https://doi.org/10.4236/ojg.2017.710103

Jin, X., Liu, C., Zhang, H., Zhou, C., Jiang, X., Wu, Z., & Xu, J. (2018). Evolutionary driven of Gephyrocapsa coccolith isotopic vital effects over the past 400 ka. *Earth and Planetary Science Letters*, *503*, 236–247. https://doi.org/10.1016/j.epsl.2018.09.010

Karas, C., Nurnberg, D., Bahr, A., Groeneveld, J., Herrle, J. O., Tiedemann, R., & deMenocal, P. B. (2017). Pliocene oceanic seaways and global climate. *Scientific Reports*, *7*(1), 39842. https://doi.org/10.1038/srep39842

Karatsolis, B., Lougheed, B. C., De Vleeschouwer, D., & Henderiks, J. (2022). Abrupt conclusion of the late Miocene-early Pliocene biogenic bloom at 4.6-4.4 Ma. *Nature Communications*, *13*(1), 353. https://doi.org/10.1038/s41467-021-27784-6

Klaas, C., & Archer, D. E. (2002). Association of sinking organic matter with various types of mineral ballast in the deep sea: Implications for the rain ratio. *Global Biogeochemical Cycles*, *16*(4), 63-61–63-14. https://doi.org/10.1029/2001gb001765

Kodama, K. P., & Hinnov, L. (2014). *Rock magnetic cyclostratigraphy*. John Wiley & Sons.

Kohfeld, K., Graham, R., De Boer, A., Sime, L., Wolff, E., Le Quéré, C., & Bopp, L. (2013). Southern Hemisphere westerly wind changes during the Last Glacial Maximum: Paleo-data synthesis. *Quaternary Science Reviews*, *68*, 76–95. https://doi.org/10.1016/j.quascirev.2013.01.017

Kohfeld, K. E., Le Quere, C., Harrison, S. P., & Anderson, R. F. (2005). Role of marine biology in glacial-interglacial CO_2 cycles. *Science*, *308*(5718), 74–78. https://doi.org/10.1126/science.1105375

Laskar, J., Fienga, A., Gastineau, M., & Manche, H. (2011). La2010: A new orbital solution for the long-term motion of the Earth. *Astronomy and Astrophysics*, *532*, 15. https://doi.org/10.1051/0004-6361/201116836

LeVay, L. J. (2024). Bulk calcium carbonate record at IODP Site U1475 during the early Pliocene [Dataset]. *Zenodo*. https://zenodo.org/records/14291394

Li, M., Hinnov, L., & Kump, L. (2019). Acycle: Time-series analysis software for paleoclimate research and education. *Comput Geosci-Uk*, *127*, 12–22. https://doi.org/10.1016/j.cageo.2019.02.011

Lisiecki, L. E., & Raymo, M. E. (2005). A Pliocene-Pleistocene stack of 57 globally distributed benthic δ18O records. *Paleoceanography*, *20*(1). https://doi.org/10.1029/2004pa001071

Lutjeharms, J. (1996). *The exchange of water between the South Indian and South Atlantic Oceans, The South Atlantic* (pp. 125–162). Springer.

Lutjeharms, J. (2006). The agulhas current. *African Journal of Marine Science*, *28*, 729–732.

Lyle, M., Drury, A. J., Tian, J., Wilkens, R., & Westerhold, T. (2019). Late Miocene to Holocene high-resolution eastern equatorial Pacific carbonate records: Stratigraphy linked by dissolution and paleoproductivity. *Climate of the Past*, *15*(5), 1715–1739. https://doi.org/10.5194/cp-15-1715-2019

Ma, Y., Weldeab, S., Schneider, R. R., Andersen, N., Garbe-Schönberg, D., & Friedrich, T. (2021). Strong Southern African monsoon and weak Mozambique channel throughflow during Heinrich events: Implication for Agulhas leakage. *Earth and Planetary Science Letters*, *574*, 117148. https://doi.org/10.1016/j.epsl.2021.117148

Mann, M. E., & Lees, J. M. (1996). Robust estimation of background noise and signal detection in climatic time series. *Climatic Change*, *33*(3), 409–445. https://doi.org/10.1007/bf00142586

Margalef, R. (1978). Life-forms of phytoplankton as survival alternatives in an unstable environment. *Oceanologica Acta*, *1*, 493–509.

Martínez-García, A., Sigman, D. M., Ren, H., Anderson, R. F., Straub, M., Hodell, D. A., et al. (2014). Iron fertilization of the Subantarctic Ocean during the last ice age. *Science*, *343*(6177), 1347–1350. https://doi.org/10.1126/science.1246848

McClelland, H. L., Barbarin, N., Beaufort, L., Hermoso, M., Ferretti, P., Greaves, M., & Rickaby, R. E. (2016). Calcification response of a key phytoplankton family to millennial-scale environmental change. *Scientific Reports*, *6*(1), 34263. https://doi.org/10.1038/srep34263

Molnar, P., England, P., & Martinod, J. (2010). Mantle dynamics, uplift of the Tibetan Plateau, and the Indian Monsoon. *Reviews of Geophysics*, *31*(4), 357–396. https://doi.org/10.1029/93rg02030

Mortlock, R. A., & Froelich, P. N. (1989). A simple method for the rapid determination of biogenic opal in pelagic marine sediments. *Deep-Sea Research, Part A: Oceanographic Research Papers*, *36*(9), 1415–1426. %@ 0198-0149. https://doi.org/10.1016/0198-0149(89)90092-7

Narciso, A., Cachão, M., & de Abreu, L. (2006). Coccolithus pelagicus subsp. pelagicus versus Coccolithus pelagicus subsp. braarudii (Coccolithophore, Haptophyta): A proxy for surface subarctic Atlantic waters off Iberia during the last 200 kyr. *Marine Micropaleontology*, *59*(1), 15–34. https://doi.org/10.1016/j.marmicro.2005.12.001

O'Dea, S. A., Gibbs, S. J., Bown, P. R., Young, J. R., Poulton, A. J., Newsam, C., & Wilson, P. A. (2014). Coccolithophore calcification response to past ocean acidification and climate change. *Nature Communications*, *5*(1), 5363. https://doi.org/10.1038/ncomms6363

Orsi, A. H., Whitworth, T., & Nowlin, W. D. (1995). On the meridional extent and fronts of the Antarctic Circumpolar Current. *Deep Sea Research Part I: Oceanographic Research Papers*, *42*(5), 641–673. https://doi.org/10.1016/0967-0637(95)00021-w

Paasche, E. (1964). A tracer study of the inorganic carbon uptake during coccolith Formation and photosynthesis in the coccolithophorid Coccolithus huxleyi. *Physiologia Plantarum*, *Suppl*., 5–82.

Parente, A., Cachao, M., Baumann, K. H., de Abreu, L., & Ferreira, J. (2004). Morphometry of Coccolithus pelagicus s.l. (Coccolithophore, Haptophyta) from offshore Portugal, during the last 200 kyr. *Micropaleontology*, *50*(Suppl_1), 107–120. https://doi.org/10.2113/50.suppl_1.107

Patil, S. M., Mohan, R., Shetye, S. S., Gazi, S., Baumann, K.-H., & Jafar, S. (2017). Biogeographic distribution of extant Coccolithophores in the Indian sector of the Southern Ocean. *Marine Micropaleontology*, *137*, 16–30. https://doi.org/10.1016/j.marmicro.2017.08.002

Patil, S. M., Mohan, R., Shetye, S. S., Gazi, S., Choudhari, P., & Jafar, S. (2020). Interannual changes of austral summer coccolithophore assemblages and southward expanse in the Southern Indian Ocean. *Deep Sea Research Part II: Topical Studies in Oceanography*, *178*, 104765. https://doi.org/10.1016/j.dsr2.2020.104765

Poulton, A. J., Adey, T. R., Balch, W. M., & Holligan, P. M. (2007). Relating coccolithophore calcification rates to phytoplankton community dynamics: Regional differences and implications for carbon export. *Deep Sea Research Part II: Topical Studies in Oceanography*, *54*(5–7), 538–557. %@ 0967-0645. https://doi.org/10.1016/j.dsr2.2006.12.003

Reid, J. L. (2005). On the world-wide circulation of the deep water from the North Atlantic Ocean. *Journal of Marine Research*, *63*(1), 187–201. https://doi.org/10.1357/0022240053693833

Romero, O. E., Kim, J. H., Bárcena, M. A., Hall, I. R., Zahn, R., & Schneider, R. (2015). High-latitude forcing of diatom productivity in the southern Agulhas Plateau during the past 350 kyr. *Paleoceanography*, *30*(2), 118–132. https://doi.org/10.1002/2014pa002636

Rost, B., & Riebesell, U. (2004). Coccolithophores and the biological pump: Responses to environmental changes. In *Coccolithophores: From molecular processes to global impact* (pp. 99–125).

Salzmann, U., Williams, M., Haywood, A. M., Johnson, A. L. A., Kender, S., & Zalasiewicz, J. (2011). Climate and environment of a Pliocene warm world. *Palaeogeography, Palaeoclimatology, Palaeoecology*, *309*(1–2), 1–8. https://doi.org/10.1016/j.palaeo.2011.05.044

Schott, F. A., Xie, S. P., & McCreary, J. P. J. P., Jr.Jr. (2009). Indian Ocean circulation and climate variability. *Reviews of Geophysics*, *47*(1). https://doi.org/10.1029/2007rg000245

Sigman, D. M., Altabet, M. A., Francois, R., McCorkle, D. C., & Gaillard, J. F. (1999). The isotopic composition of diatom-bound nitrogen in Southern Ocean sediments. *Paleoceanography*, *14*(2), 118–134. https://doi.org/10.1029/1998pa900018

Sigman, D. M., & Boyle, E. A. (2000). Glacial/interglacial variations in atmospheric carbon dioxide. *Nature*, *407*(6806), 859–869. https://doi.org/10.1038/35038000

Takahashi, K., & Okada, H. (2000). The paleoceanography for the last 30,000 years in the southeastern Indian Ocean by means of calcareous nannofossils, Mar Micropaleontol. *Marine Micropaleontology*, *40*(1–2), 83–103. https://doi.org/10.1016/s0377-8398(00)00033-5

Tangunan, D., Berke, M. A., Cartagena-Sierra, A., Flores, J. A., Gruetzner, J., Jimenez-Espejo, F., et al. (2021). Strong glacial-interglacial variability in upper ocean hydrodynamics, biogeochemistry, and productivity in the southern Indian Ocean. *Communications Earth & Environment*, *2*(1), 80. https://doi.org/10.1038/s43247-021-00148-0

Tangunan, D., Flores, J.-A., & Fuertes, M. A. (2024). Reticulofenestra morphometry at IODP Site U1475 during the early Pliocene [Dataset]. *Zenodo*. https://zenodo.org/records/14291319

Tangunan, D., Flores, J.-A., & LeVay, L. J. (2024). Absolute and relative abundances of calcareous nannofossils at IODP Site U1475 during the early Pliocene [Dataset]. *Zenodo*. https://zenodo.org/records/14291181

Taylor, A. K., Berke, M. A., Castañeda, I. S., Koutsodendris, A., Campos, H., Hall, I. R., et al. (2021). Plio-pleistocene continental hydroclimate and Indian ocean sea surface temperatures at the southeast African Margin. *Paleoceanography and Paleoclimatology*, *36*(3). https://doi.org/10.1029/2020pa004186

Thomson, D. J. (1982). Spectrum estimation and harmonic analysis. *Proceedings of the IEEE*, *70*(9), 1055–1096. https://doi.org/10.1109/proc.1982.12433

Tian, J., Xie, X., Ma, W., Jin, H., & Wang, P. (2011). X-ray fluorescence core scanning records of chemical weathering and monsoon evolution over the past 5 Myr in the southern South China Sea. *Paleoceanography*, *26*(4). https://doi.org/10.1029/2010pa002045

Tim, N., Zorita, E., Emeis, K.-C., Schwarzkopf, F. U., Biastoch, A., & Hünicke, B. (2019). Analysis of the position and strength of westerlies and trades with implications for Agulhas leakage and South Benguela upwelling. *Earth System Dynamics*, *10*(4), 847–858. https://doi.org/10.5194/esd-10-847-2019

Tim, N., Zorita, E., Hünicke, B., & Ivanciu, I. (2023). The impact of the Agulhas Current system on precipitation in southern Africa in regional climate simulations covering the recent past and future. *Weather and Climate Dynamics*, *4*(2), 381–397. https://doi.org/10.5194/wcd-4-381-2023

Tréguer, P. (2002). Silica and the cycle of carbon in the ocean. *Comptes Rendus Geoscience*, *334*(1), 3–11. https://doi.org/10.1016/s1631-0713(02)01680-2

Villa, G., Fioroni, C., Persico, D., Roberts, A. P., & Florindo, F. (2014). Middle Eocene to Late Oligocene Antarctic glaciation/deglaciation and Southern Ocean productivity. *Paleoceanography*, *29*(3), 223–237. https://doi.org/10.1002/2013pa002518

Winter, A., Jordan, R. W., & Roth, P. H. (1994). Biogeography of living coccolithophores in ocean waters. In A. Winter & W. G. Siesser (Eds.), *Coccolithophores* (p. 37). Cambridge University Press.

Xulu, N. G., Chikoore, H., Bopape, M.-J. M., & Nethengwe, N. S. (2020). Climatology of the Mascarene high and its influence on weather and climate over southern Africa. *Climate*, *8*(7), 86. https://doi.org/10.3390/cli8070086

Young, J. (1990). Size variation of Neogene Reticulofenestra coccoliths from Indian Ocean DSDP cores. *Journal of Micropalaeontology*, *9*(1), 15–85. https://doi.org/10.1144/jm.9.1.71

Young, J. (1998). Neogene. In P. R. Bown (Ed.), *Calcareous nannofossil biostratigraphy* (1st ed., pp. 225–265). Chapman & Hall.

Young, J., Henriksen, K., & Probert, I. (2004). Structure and morphogenesis of the coccoliths of the CODENET species. In *Coccolithophores: From molecular processes to global impact* (pp. 191–216).

Young, J. R., & Ziveri, P. (2000). Calculation of coccolith volume and its use in calibration of carbonate flux estimates. *Deep-Sea Res Pt*, *Ii*, 1679–1700.

Zachos, J., Pagani, M., Sloan, L., Thomas, E., & Billups, K. (2001). Trends, rhythms, and aberrations in global climate 65 Ma to present. *Science*, *292*(5517), 686–693. https://doi.org/10.1126/science.1059412

Zhang, L., Chen, M., Xiang, R., Zhang, L., & Lu, J. (2009). Productivity and continental denudation history from the South China Sea since the late Miocene. *Marine Micropaleontology*, *72*(1–2), 76–85.

Zhang, Y. G., Ji, J., Balsam, W., Liu, L., & Chen, J. (2009). Mid-Pliocene Asian monsoon intensification and the onset of Northern Hemisphere glaciation. *Geology*, *37*(7), 599–602. https://doi.org/10.1130/g25670a.1